REPORT DOCUMENTATION PAGE

Form Approved
OMB No. 0704-0188

1. REPORT DATE *(DD-MM-YYYY)*	**2. REPORT TYPE**	**3. DATES COVERED** *(From - To)*
29-11-2010	Technical Paper	

4. TITLE AND SUBTITLE

Far-Field Plume Measurements of a Nested-Channel Hall-Effect Thruster

5a. CONTRACT NUMBER

5b. GRANT NUMBER

5c. PROGRAM ELEMENT NUMBER

6. AUTHOR(S)
Raymond Liang and Alec D. Gallimore (University of Michigan)

5d. PROJECT NUMBER

5e. TASK NUMBER

5f. WORK UNIT NUMBER
33SP0708

7. PERFORMING ORGANIZATION NAME(S) AND ADDRESS(ES)

University of Michigan
500 S. State Street
Ann Arbor MI 48109

8. PERFORMING ORGANIZATION REPORT NUMBER

AFRL-RZ-ED-TP-2010-523

9. SPONSORING / MONITORING AGENCY NAME(S) AND ADDRESS(ES)

Air Force Research Laboratory (AFMC)
AFRL/RZS
5 Pollux Drive
Edwards AFB CA 93524-7048

10. SPONSOR/MONITOR'S ACRONYM(S)

11. SPONSOR/MONITOR'S NUMBER(S)
AFRL-RZ-ED-TP-2010-523

12. DISTRIBUTION / AVAILABILITY STATEMENT

Distribution A: Approved for public release; distribution unlimited (PA #10627).

13. SUPPLEMENTARY NOTES
For presentation at the 49th AIAA Aerospace Sciences Conference, Orlando, FL, 04-07 Jan 2011.

14. ABSTRACT

Far-field plume measurements were performed on the X2 nested-channel Hall-effect thruster using an array of diagnostics, including a nude Faraday probe, retarding potential analyzer, and ExB probe. Data from these probes were used to calculate utilization efficiencies from existing efficiency models in order to investigate various phenomena that contribute to the total efficiency of the X2. Comparisons of utilization efficiencies show an increase in voltage utilization and a slight decrease in charge utilization when both channels operate simultaneously (nested-channel mode). Mass utilization, current utilization, and beam divergence were approximately the same between operation of individual channels and operation of both channels. Given the results of the far-field diagnostics, a nested-channel Hall effect thruster has been shown to operate much like a conventional Hall thruster when both available channels are at the same discharge voltage. Small improvements in performance in the nested-channel mode are likely due to reduced cathode-coupling voltage and better acceleration of ions.

15. SUBJECT TERMS

16. SECURITY CLASSIFICATION OF:			**17. LIMITATION OF ABSTRACT**	**18. NUMBER OF PAGES**	**19a. NAME OF RESPONSIBLE PERSON**
					Dr. Daniel Brown
a. REPORT	**b. ABSTRACT**	**c. THIS PAGE**	SAR	49	**19b. TELEPHONE NUMBER** *(include area code)*
Unclassified	**Unclassified**	**Unclassified**			N/A

Far-Field Plume Measurements of a Nested-Channel Hall-Effect Thruster

Raymond Liang* and Alec D. Gallimore†
University of Michigan, Ann Arbor, MI, 48109, USA

Far-field plume measurements were performed on the X2 nested-channel Hall-effect thruster using an array of diagnostics, including a nude Faraday probe, retarding potential analyzer, and E×B probe. Data from these probes were used to calculate utilization efficiencies from existing efficiency models in order to investigate various phenomena that contribute to the total efficiency of the X2. Comparisons of utilization efficiencies show an increase in voltage utilization and a slight decrease in charge utilization when both channels operate simultaneously (nested-channel mode). Mass utilization, current utilization, and beam divergence were approximately the same between operation of individual channels and operation of both channels. Given the results of the far-field diagnostics, a nested-channel Hall effect thruster has been shown to operate much like a conventional Hall thruster when both available channels are at the same discharge voltage. Small improvements in performance in the nested-channel mode are likely due to reduced cathode-coupling voltage and better acceleration of ions.

Nomenclature

A_c	= collector area
I_{axial}	= axial beam current
I_b	= beam current
I_d	= discharge current
$\dot{m}_a$	= anode mass flow rate
$\dot{m}_c$	= cathode mass flow rate
$\dot{m}_t$	= total mass flow rate
N	= number of nested channels
Q	= average charge of ions
P_d	= discharge power
P_t	= total power
R	= radial position
R_{CL}	= channel centerline radius
R_L	= distance to left side of channel
R_R	= distance to right side of channel
T	= thrust
V_a	= acceleration voltage
V_c	= cathode coupling voltage
V_d	= discharge voltage
V_{mp}	= most-probable voltage
V_p	= plasma potential
Z	= charge state
α_L	= left incidence angle
α_R	= right incidence angle
β	= plume divergence half-angle
η_b	= current utilization efficiency
η_c	= cathode efficiency
η_d	= divergence efficiency
η_m	= mass utilization efficiency
η_{mag}	= electromagnet efficiency
η_q	= charge utilization efficiency
η_t	= total efficiency
η_v	= voltage utilization efficiency
θ	= angular position from thruster centerline
κ_A	= area correction factor
κ_D	= distance correction factor
κ_G	= gap correction factor
Ω	= ion species current fraction

*Ph.D. Candidate, Aerospace Engineering, rayliang@umich.edu, and Student Member, AIAA.
†Arthur F. Thurnau Professor, Aerospace Engineering, alec.gallimore@umich.edu, and Fellow, AIAA.

I. Introduction

The Plasmadynamics and Electric Propulsion Laboratory (PEPL) at the University of Michigan, with the support of the Air Force Research Laboratory, has developed and tested a laboratory-model nested-channel Hall-effect thruster (NHT). Named the X2, the Hall thruster was developed to determine the capabilities of the nested-channel configuration. The X2 features two concentric discharge channels with a shared internal cathode, as shown in Figure 1. Nesting is a relatively unexplored concept of clustering discharge channels of a Hall thruster. Available literature shows mostly conceptual consideration for nested-channel configuration with only a single mention of a development effort.[1–3] Prior to the X2, the performance of a nested-channel Hall thruster has never been published, and the potential advantages have never been evaluated. Additionally, the properties of the plume of a nested-channel Hall thruster have never been determined and compared to those of traditional Hall thrusters.

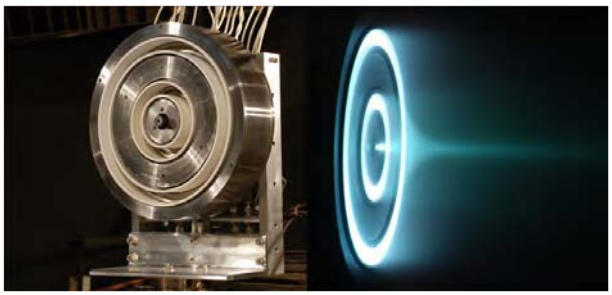

Figure 1: X2 nested-channel Hall-effect thruster

The nested-channel configuration has a number of advantages that make it particularly suitable for high-power electric propulsion. Studies have shown that nesting channels can lead to significant reductions in thruster mass and footprint area.[1,4] Additionally, the nested-channel configuration has the ability to change the exit area through the selective activation of available channels, which provides an additional method of throttling and a means of efficiently adapting to various levels of available spacecraft power. Multiple discharge channels also give a degree of system redundancy and permit multiple design points for the overall thruster.

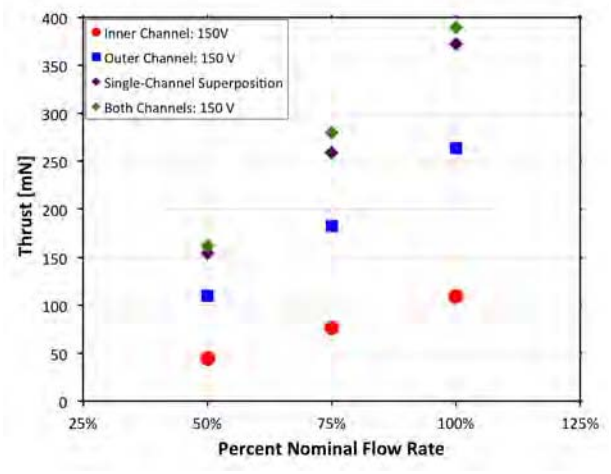

Figure 2: Comparison of thrusts from single-channel and nested-channel modes at constant background pressure

Operation of the X2 with each channel firing individually (single-channel mode) and two channels firing simultaneously (nested-channel mode) has already been demonstrated and preliminary performance measurements have been reported. Slight improvements in performance in nested-channel mode were observed in previous measurements, although the cause of the increased thrust was unknown. Facility effects were eliminated as a possibility after single-channel operating conditions were conducted at the same background pressure as the corresponding nested-channel condition, as shown in Figure 2. The nested-channel thrusts were still approximately 5% greater than the superposition single-channel thrusts when the applied magnetic fields and cathode flow fractions were held constant. Additional measurements to further investigate the nested-channel mode of the X2 were natural and necessary.

The purpose of this study is to investigate how the operating characteristics of the X2 change from single-channel mode to nested-channel mode by utilizing a traditional array of far-field diagnostics, which include a nude Faraday probe, retarding potential analyzer (RPA), and E×B probe. To the knowledge of the authors, measurements using these diagnostics have never been taken and reported for a nested-channel Hall thruster.

Measurements from these probes are used to determine five utilization efficiencies that are part of existing efficiency models for Hall thrusters.[5,6] The five efficiencies are:

- Current utilization efficiency, η_b
- Divergence efficiency, η_d
- Charge utilization efficiency, η_q
- Voltage utilization efficiency, η_v
- Mass utilization efficiency, η_m

The total efficiency, η_t, of a Hall thruster can be broken down into the utilization efficiencies by the following equation:

$$\eta_t = \frac{T^2}{2\dot{m}_t P_t} = \eta_b \eta_d \eta_q \eta_v \eta_m \eta_{mag} \tag{1}$$

where the electromagnet efficiency, η_{mag}, is the ratio of the discharge power to the total power, P_d/P_t.

Current density profiles from a Faraday probe were used to calculate divergence efficiency, current utilization efficiency, and mass utilization efficiency. The current fractions from the measured spectra of the E×B probe were used to determine charge utilization efficiency and mass utilization efficiency. Measurements of the RPA and an adjacent Langmuir probe (LP) were used to determined voltage utilization efficiency.

II. Methodology for Calculation of Parameters

A. Current Utilization

$$\eta_b = \frac{I_b}{I_d} \tag{2}$$

$$I_b = 2\pi R^2 \int_0^{\frac{\pi}{2}} \frac{I(\theta,R)}{A_c + \kappa_G} \frac{\kappa_D(\theta,R,R_{CL_1},R_{CL_2})}{\kappa_A(\theta,R,R_{CL_1},R_{CL_2})} \sin(\theta) d\theta \tag{3}$$

η_b is the ratio of the beam current to the discharge current, as shown in Equation 2, and is a measure of how much of the input current is carried by thrust-producing ions. Discharge current is directly measured using current shunts. Beam current is calculated by hemispherical integration of the azimuthal distribution of ion current density as measured by a Faraday probe. The full expression for I_b is shown in Equation 3. Corrections for the collection area A_c and the radial position R, as described by Brown and Gallimore, were implemented in this study to improve the accuracy of the nude Faraday probe measurements.[7,8]

κ_G is the gap correction factor and accounts for ion current collection along the side-walls of the Faraday probe collector. The area correction factor, κ_A, corrects for the cosine losses due to the annular geometry of the ion source. The distance correction factor, κ_D, corrects for the error in radial distance R from the annular ion source, as R is measured with respect to thruster centerline and not with respect to the channels. However, the original formulations of κ_A and κ_D were meant for a single-channel Hall thrusters. For use with the X2 in nested-channel mode, the correction factors were modified to include both annular ion sources.

$$\kappa_A = \cos^2\left[\frac{\sum_{i=1}^{N}(\alpha_{L_i} + \alpha_{R_i})I_{d_i}}{2\sum_{i=1}^{N} I_{d_i}}\right] \tag{4}$$

$$\alpha_{L_i,R_i} = \mp\theta \mp \tan^{-1}\left(\frac{-\sin(\theta) - \frac{R_{CL_i}}{R}}{\cos(\theta)}\right) \tag{5}$$

α_{L_i,R_i} are angles of incidence from the left and right sides, respectively, of the ith of N total annuli in the plane of actuation of the Faraday probe. For the X2, N is 2. The angles of incidence to each channel are weighted by the corresponding discharge current I_{d_i} so that κ_A is biased toward its value for the channel that dominates I_b. If the current

from one of two channels goes to zero, the single-channel κ_A is recovered for the other channel. This allows κ_A to be remain valid regardless of X2's operating mode. Discharge currents are used in the weighting instead of beam currents because far-field Faraday probe measurements are unable to distinguish between the individual ion beams.

$$\kappa_D = \left[\frac{\sum_{i=1}^{N} \left(\frac{R_{L_i}}{R} + \frac{R_{R_i}}{R} \right) I_{d_i}}{2 \sum_{i=1}^{2} I_{d_i}} \right] \tag{6}$$

$$\frac{R_{L_i,R_i}}{R} = \sqrt{[\cos(\theta)]^2 + \left[-\sin(\theta) \mp \frac{R_{CL_i}}{R} \right]^2} \tag{7}$$

κ_D was similarly modified to include both channels. The normalized distances $R_{L_i,R_i}/R$ are also weighted by the corresponding discharge current, biasing the correction factor κ_D toward that of the dominant channel. For the X2 in single-channel mode, the zero discharge current of one channel results in the recovery of original formulation κ_D as applied to the active channel.

B. Divergence

$$\eta_d = [\cos(\beta)]^2 = \left(\frac{I_{axial}}{I_b} \right)^2 \tag{8}$$

$$\beta = \cos^{-1} \left(\frac{I_{axial}}{I_b} \right) \tag{9}$$

$$I_{axial} = 2\pi R^2 \int_0^{\frac{\pi}{2}} \frac{I(\theta,R)}{A_c + \kappa_G} \frac{\kappa_D(\theta,R,R_{CL_1},R_{CL_2})}{\kappa_A(\theta,R,R_{CL_1},R_{CL_2})} \cos(\theta)\sin(\theta) d\theta \tag{10}$$

The parameter η_d describes the degree of collimation in the ion beam from the Hall thruster and is related to the plume divergence half-angle β by Equation 8.[6] β is calculated by using the ratio of axial beam current, I_{axial}, to total beam current, I_b, as shown in Equation 9. I_{axial}, as expressed in Equation 10, is determined in a manner similar to the calculation of I_b with an addition factor to account for the orientation of the probe.

C. Charge Utilization

$$\eta_q = \frac{\left(\sum_{i=1}^{n} \frac{\Omega_i}{\sqrt{Z_i}} \right)^2}{\sum_{i}^{n} \frac{\Omega_i}{Z_i}} \tag{11}$$

Charge utilization efficiency η_q, as defined in Equation 11, describes the composition of the plume in terms of the charge states of the ions. η_q is unity if all ions are singly-charged and, when less than unity, reflects "over-ionization" due to the presence of multiply-charged ions.

The current fraction of the ith ion species, Ω_i, is determined from an E×B probe trace by the methods outlined by Shastry *et al.*[9] Specifically, the triangle method and simplified charge exchange model are used in this study to calculate Ω_i. Z_i is the ion charge state. For the purposes of this study, values for Z_i greater than 4 are not considered, as quadruply-charged current fractions are already very small and on the order of the associated uncertainty.

D. Voltage Utilization

$$\eta_v = \frac{V_a}{V_d} = \frac{V_{mp} - V_p}{V_d} = 1 - \frac{V_c}{V_d} \tag{12}$$

Voltage utilization efficiency, η_v, is the fraction of the discharge voltage is used for acceleration of ions, as described in Equation 12. The fraction of the discharge voltage not used for acceleration of ions is used to extract electrons from the cathode, and the corresponding voltage is known as the cathode coupling voltage, V_c.

The accelerating voltage, V_a, is determined by methods outlined by Hofer.[10] RPA traces are numerically differentiated and the voltage corresponding to the maximum in the differentiated signal is known as the most-probable voltage, V_{mp}. Using an adjacent Langmuir probe, the local plasma potential, V_P is determined by finding the voltage of the characteristic "knee" in the I-V characteristic. As shown in Equation 12, the most-probable voltage is corrected by the plasma potential to calculate the accelerating voltage.

E. Mass Utilization

$$\eta_m = \frac{m_{Xe} I_d}{\dot{m}_t e} \eta_b \sum_{i=1}^{n} \frac{\Omega_i}{Z_i} = \frac{m_{Xe} I_b}{\dot{m}_t e Q} \tag{13}$$

Mass utilization efficiency is the fraction of the supplied propellant mass flow that is converted into ions, as described in Equation 13. η_m is the only parameter that is not directly measured by a probe but uses FP and E×B measurements to estimate mass flow. The mass flow of ions is calculated from the ion beam current, $I_b = I_d \eta_b$, and the mass-to-average charge ratio of ions, m_{Xe}/eQ.

It should be noted that the definition of η_m used in Equation 13 is from work performed by Brown *et al* and differs from prior definitions in that the mass flow rate in the denominator is the total mass flow, $\dot{m}_t$, instead of the anode mass flow, $\dot{m}_a$. However, the definition of η_t remains consistent, as the cathode efficiency, $\eta_c = \dot{m}_a/\dot{m}_t$, is absorbed into this definition of η_m.

III. Experimental Apparatus

A. Nested-Channel Hall-Effect Thruster

The X2 NHT features two discharge channels with similar cross-sectional dimensions, magnetic field topologies, and gas distributors. The radial magnetic field points radially inward across the inner channel and radially outward across the outer channel. Testing of the X2 was conducted with an updated version of the internally-mounted LaB_6 hollow cathode used for a 6-kW laboratory Hall thruster. At the beginning of every pumpdown, both channels of the X2 were operated for a bake-out period of one hour.

Both anodes and the cathode had separate stainless steel propellant feed lines. MKS Model 1179A mass flow controllers were used to regulate propellant flow through the outer anode and the cathode, and an MKS Model 1159B mass flow controller was used for the inner anode. All three mass flow controllers were connected to an MKS Model 247C 4-channel readout. The manufacturer-specified accuracy of the mass flow controllers is 1% of full scale. Research grade xenon at 99.999% purity was used throughout testing.

Electrical connections for the X2 were made such that each channel had a separate discharge power supply and the common for both discharge circuits was connected to the shared internal cathode. This electrical configuration was based on previous work performed at PEPL on clustered Hall thrusters with a shared hollow cathode.[11,12] The thruster was electrically grounded to the facility ground during testing.

The inner channel discharge was powered by a Sorensen PRO 600-16T while the outer channel discharge was powered by an American Reliance HPS 1000-100-K027. Power for the magnets were provided by three EMI EMS 60-10 power supplies and one EMI EMS 100-10. The two trim coils were powered by a Sorensen DCS 60-18E and a DCS 600-1.7. Cathode keeper power was provided by an EMI EMS 600-1.6, and heater power was provided by a Sorensen DCS 33-33.

B. Faraday Probe

The nude Faraday probe used in this study was a nested Faraday probe based on work done by Brown and Gallimore.[7,8] The collectors and guard ring are made from graphite and the ceramic shell is composed of macor. Graphite was chosen for its low secondary electron yield when bombarded with xenon, and both graphite and macor were selected for their machinability. The current collected by the inner and outer collectors were determined independently by measuring the voltage across shunt resistors with resistances of 107.1 Ω and 107.4 Ω, respectively. Both collectors were biased to -30V±0.1V with respect to facility ground by a Kikusui PAD 55-6L power supply. This voltage was found to place the collectors well within ion saturation in the plume of the X2.

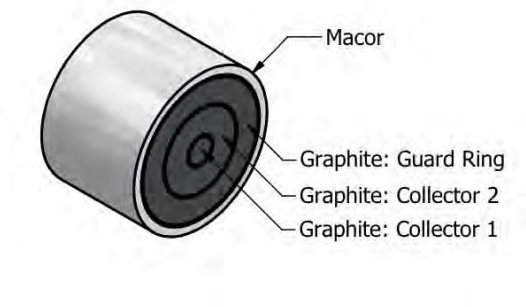

Figure 3: Nested Faraday probe

The Faraday probe was swept at a radius of 1 m from the center of the exit plane of the X2, as illustrated in Figure 4. This distance for *R* was chosen for its ubiquity in Hall thruster Faraday

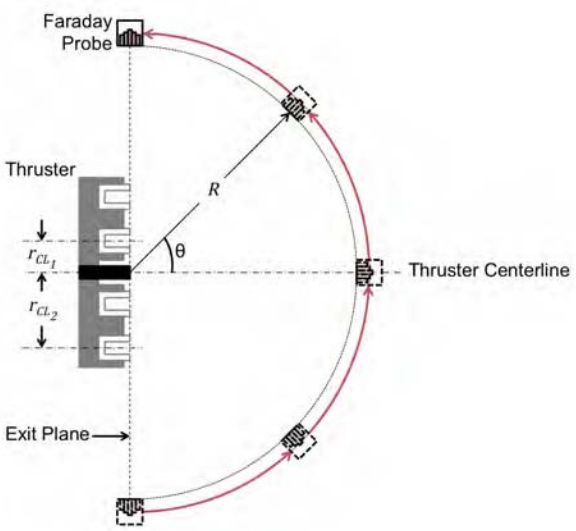

Figure 4: Faraday probe actuation

probe measurements. The coordinate system for the Faraday probe traces places the origin at the exit plane along thruster centerline so θ is zero along the thrust axis.

C. E×B Probe

The E×B probe used in this study was designed by NASA Glenn Research Center and is more thoroughly described in previous work by Reid *et al.*[13] The probe features a 150-mm test section with 75-mm entrance and exit collimators. Aperture diameters for the entrance orifice and the collimating orifices were 1.6 mm. The internal magnetic field was created by sintered hard ferrite permanent magnets, while the time-varying, internal electric field was generated by two parallel conducting plates to which voltage was applied by a Keithley 2410 Sourcemeter. Ions that passed through the test section were collected by a combined cone-and-cylinder collector that has been spray coated with tungsten to reduce secondary electron emission. Collected current was measured by a Keithley 6485 Picoammeter.

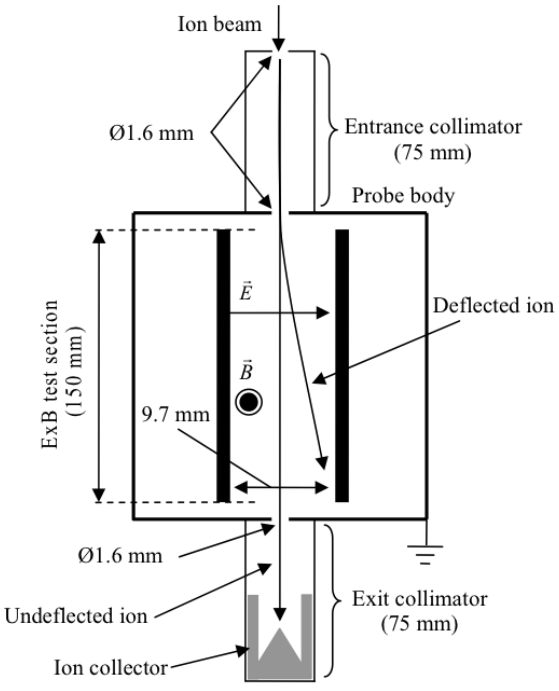

Figure 5: ExB probe schematic[9]

D. Retarding Potential Analyzer

The RPA used in this study was originally designed and built by the Air Force Research Laboratory and is described in further detail in separate documents by Reid and Hofer.[10,14] As shown in Figure 6, the grids and the collector of the RPA are separated by macor spacers which are housed within a macor sleeve and stainless steel shell. In order to repel electrons, the electron repelling grid was biased to -30V with respect to facility ground by an HP Model 721A power supply. The voltage applied ion retarding grid was swept by a Keithley 2410 Sourcemeter, and the collected current was measured by a Keithley 6485 Picoammeter.

A cylindrical Langmuir probe was placed adjacent to the RPA for the necessary measurements of local plasma potential. The Langmuir probe was composed of a 0.25-mm diameter tungsten wire that protruded 6.6 mm from a 1.5-mm diameter alumina tube.

The E×B probe, RPA, and Langmuir probe were placed 2.1 m downstream of the exit plane. The E×B probe was protected by graphite plates in front and on the plume side to prevent overheating of the probe body. The RPA was protected by a graphite shutter and the shadow of the E×B probe when the probe array was not in use. Lateral actuation was provided by a 1.5-m linear translation stage, allowing the array of probes to be placed directly downstream of the individual centerlines of the inner channel and outer channel. The lateral position uncertainty was approximately ±1 mm.

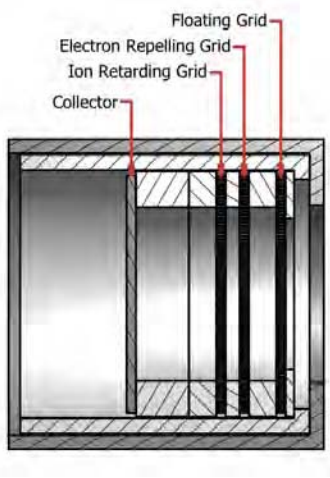

Figure 6: Retarding potential analyzer (Not to Scale)

E. Vacuum Facility

Experiments on the X2 were performed in the Large Vacuum Test Facility (LVTF) in PEPL at the University of Michigan. LVTF is a cylindrical vacuum chamber which measures 6 meters in diameter and 9 meters in length. Seven CVI model TM-1200 cryopumps with liquid nitrogen shrouds are used to achieve a base pressure of 3×10^{-7} torr. The nominal pumping speed for xenon is 245,000 l/s with all seven cryopumps operating. Pressure was measured using a Varian UHV-24 nude ionization gauge connected to a Varian XGS-600 gauge controller. Typical accuracy for a nude ionization gauge is approximately ±20% according to Varian.[15]

IV. Results

Table 1 shows the single-channel and nested-channel operating conditions during which far-field measurements were taken. In order to learn more about how the two channels combine in nested-channel mode, the inner and outer channels were operated individually under the same electromagnet settings and cathode flow fraction as the corresponding nested-channel operating condition. The single-channel operating conditions are meant to closely approximate how each channel is operating during nested-channel mode, but the influence of the adjacent plasma will naturally be missing. However, information about the interaction between channels can be gleaned from the differences in characteristics of the single-channel modes and the nested-channel modes.

This set of operating conditions is centered at the condition with the highest thrust-to-power ratio, and discharge voltage and mass flow rate were changed across this condition of interest. The discharge voltages applied to both channels are always the same during this study, and the current densities of each channel are nearly equal. The cathode flow fraction was kept constant at 10%, as this fraction was found to work well at lower flow rates and lower discharge voltages.

A. Faraday Probe

The angular current density profiles measured by the Faraday probe are shown in Figures 7(a)-8(c). Measurements from the inner and outer collectors were found to be nearly identical, so only the inner collector measurements are presented here. All profiles in Figures 7(a)-8(c) include the gap and geometric corrections as previously described.

The X2 current density profiles exhibit expected characteristics for low-voltage operation. The plume is less collimated at low discharge voltages, resulting in a more gradual falloff in current density from the core (0 deg) to the wings (±90 deg). As discharge voltage increases, plume collimation improves, and more of the beam current is carried near the core. The current density distributions are less sensitive to changes in propellant mass flow rate, as the profiles at fixed discharge voltage are similar in geometry but vertically shifted due to differences in total beam current.

As expected, the outer channel appears to dominate the combined plume, as it carries over twice the mass flow and current as the inner channel. However, the inner channel has some influence over the combined current density profile. Most of the outer-channel profiles exhibit asymmetry about the thruster centerline at 0 deg, but the asymmetries become less pronounced in the nested-channel profile. This appears to be a blending effect caused by the presence of additional ions in the core of the plume.

Table 1: X2 Operating Conditions

Discharge Voltage [V]	Anode Mass Flow Rate (Inner Channel) [mg/s]	Anode Mass Flow Rate (Outer Channel) [mg/s]
150	4.7	11.6
100	7.0	17.4
150	7.0	17.4
200	7.0	17.4
150	9.3	23.2
150	4.7	-
100	7.0	-
150	7.0	-
200	7.0	-
150	9.3	-
150	-	11.6
100	-	17.4
150	-	17.4
200	-	17.4
150	-	23.2

For reference, the superpositions of the single-channel current density profiles are included for comparison to the nested-channel current density profiles. The superpositions of single-channel profiles could potentially be used as approximations of the nested-channel profiles, but they are shown in Figures 7(a)-8(c) to consistently underestimate current density in the core while overestimating in the wings.

The calculated current utilization efficiencies from the Faraday probe measurements are shown in Figures 9(a) and 9(b). Overall, η_b increases from 100 V to 200 V and remains relatively constant with increasing flow rate at 150 V. Differences between single-channel and nested-channel values of η_b are small and practically negligible when including the measurement uncertainty. The dominant source of uncertainty for η_b is the relative uncertainty in I_b, which is 3% when available data allows for extrapolation of the current density profile to vacuum.[16] Otherwise, based on variations in I_b with and without the vacuum extrapolation, the relative uncertainty in I_b is approximately 5%. The uncertainty in I_{d_i} is estimated to be ± 0.1 A.

Divergence efficiency, as shown in Figures 10(a) and 10(b), also increases with discharge voltage and remains relatively constant with flow rate. The uncertainty in divergence efficiency is relatively high because Faraday probe traces were not taken at multiple radial distances for each of the 15 operating conditions. As a result, the relative uncertainty in the ratio of I_{axial} to I_b increases from 5% to 10%.[16]

B. E×B Probe

E×B spectra for all operating conditions are shown in Figures 11(a) to 12(c). Each individual plot compares a single-channel spectrum with a nested-channel spectrum using measurements that are most relevant to the single channel. All plots regarding to the inner channel has the E×B probe directly downstream of the inner channel, while all plots regarding the outer channel has the probe downstream of the outer channel.

The E×B spectra show expected trends with respect to discharge voltage and flow rate. Singly- and doubly-charged ions dominate at 100V, and increasing discharge voltage results in increasing current fractions of multiply-charged species. Increased flow rates also result in greater current fractions of multiply-charged species. Quadruply-charged xenon remained largely undetectable until 200 V, where Ω_4 was still approximately 0.01.

Comparisons between nested-channel and single-channel spectra reveal some additional details on nested-channel operation. Firing both channels simultaneously inherently increases the total flow rate, so the current fractions of multiply-charge species increase during nested-channel operation as they do with increasing flow rate during single-channel operation. Relative the corresponding single-channel spectrum, most of the nested-channel spectrums are also shifted to higher applied voltages. This shift in the peaks of all charge species suggests that the ions arriving from the

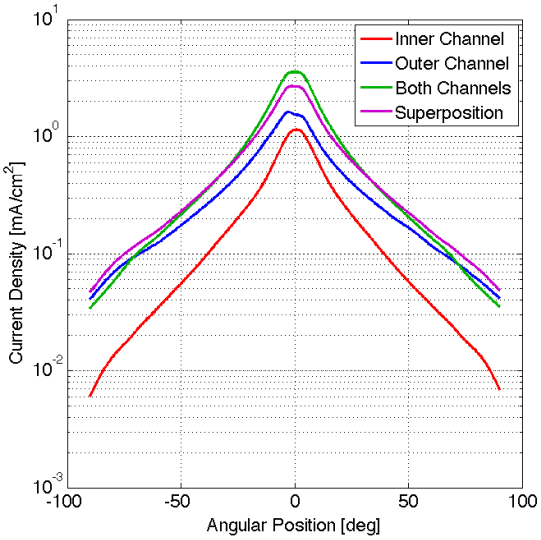

(a) Current density profiles at 100V

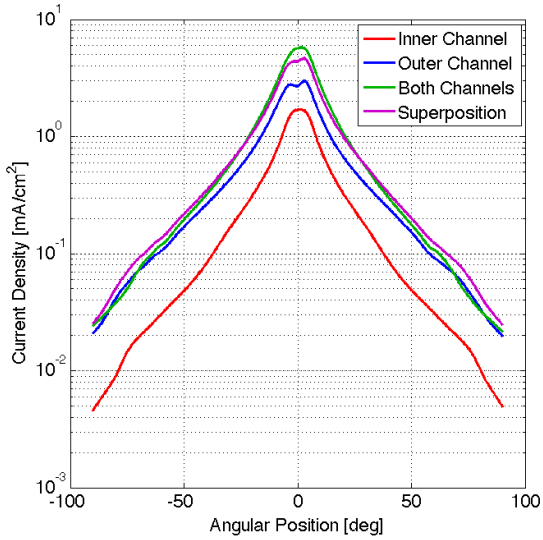

(b) Current density profiles at 150V

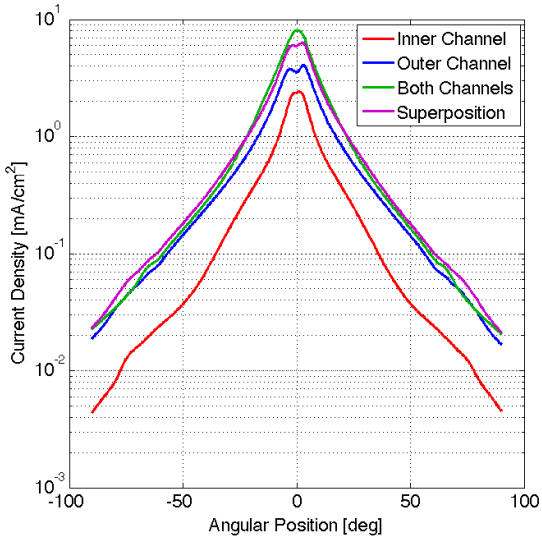

(c) Current density profiles at 200V

Figure 7: Single-channel and nested-channel current density profiles at fixed flow rate

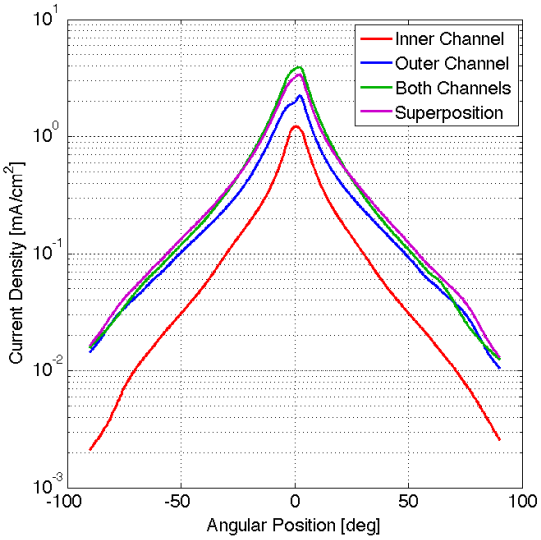

(a) Current density profiles at 50% nominal flow rate

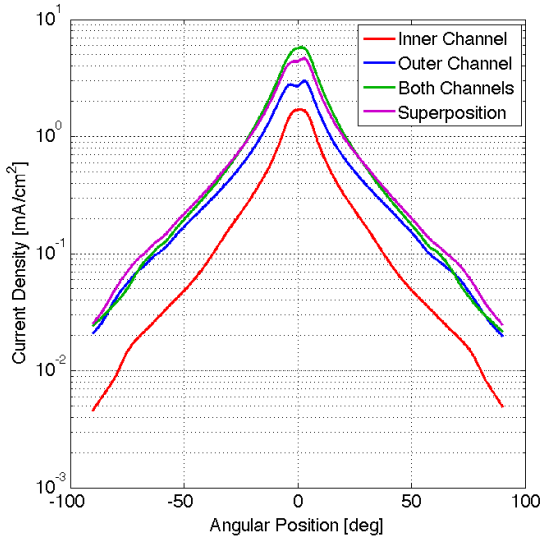

(b) Current density profiles at 75% nominal flow rate

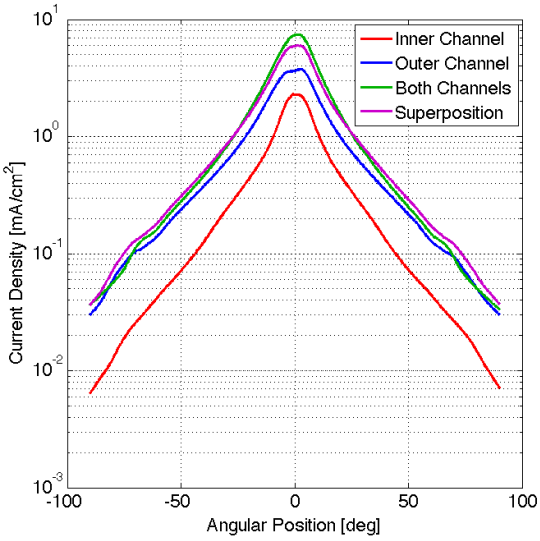

(c) Current density profiles at 100% nominal flow rate

Figure 8: Single-channel and nested-channel current density profiles at fixed discharge voltage

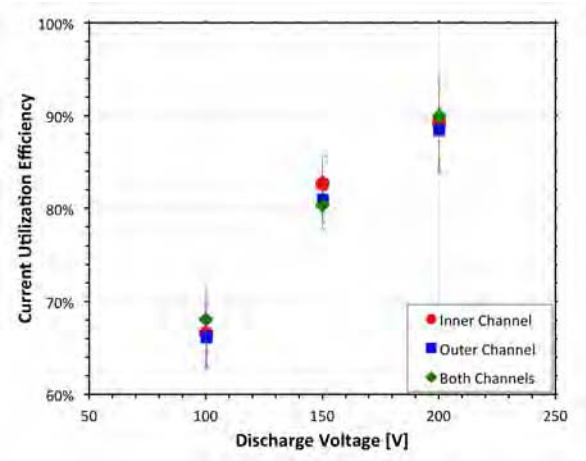

(a) Current utilization efficiency variation with voltage

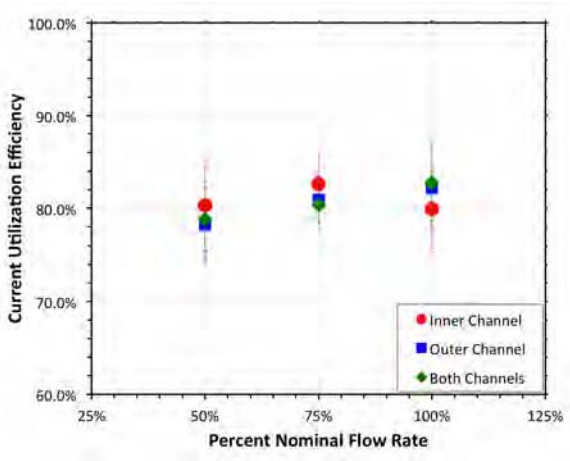

(b) Current utilization efficiency variation with mass flow rate

Figure 9: Current utilizations efficiencies

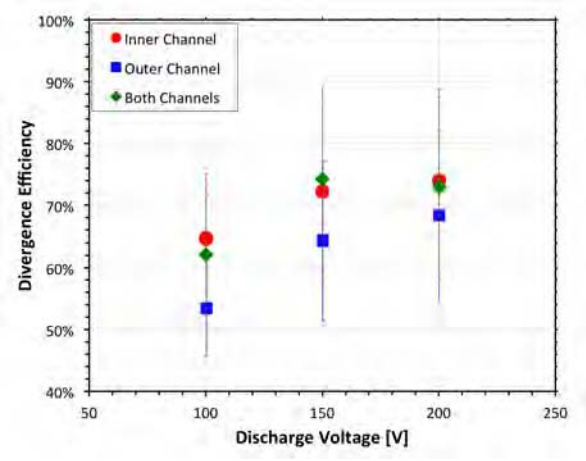

(a) Divergence efficiency variation with voltage

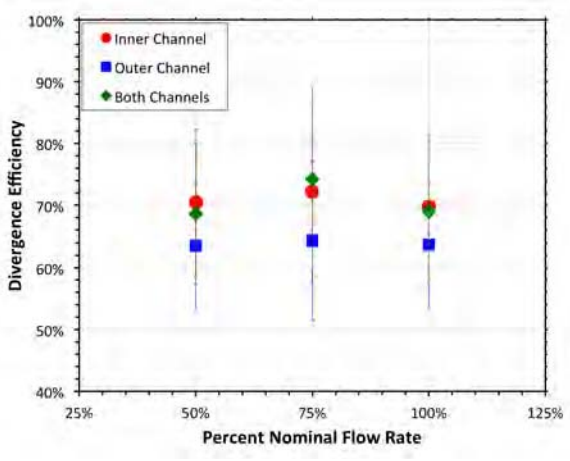

(b) Divergence efficiency variation with mass flow rate

Figure 10: Divergence efficiencies

thruster are moving faster during nested-channel operation.

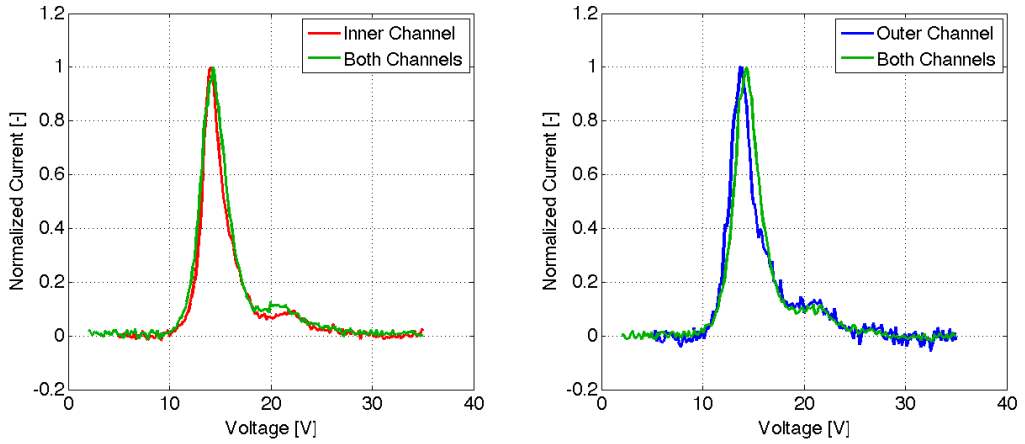

(a) E×B probe spectra at 100V

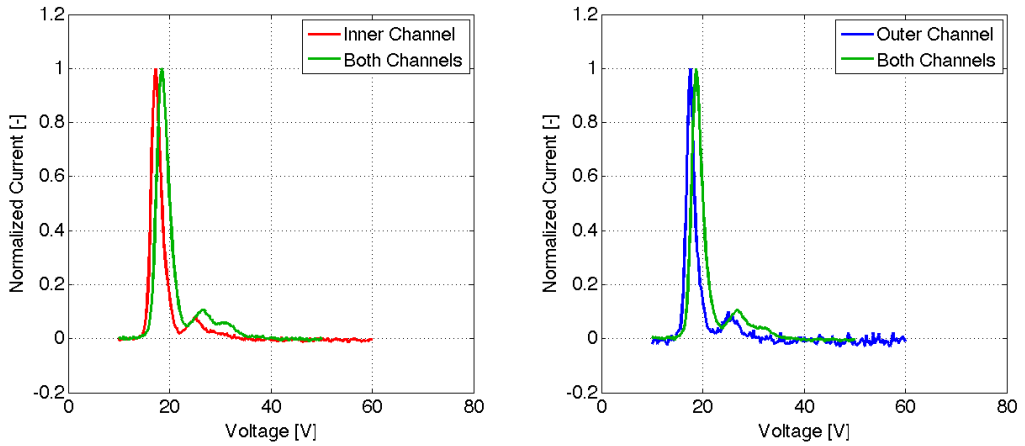

(b) E×B probe spectra at 150V

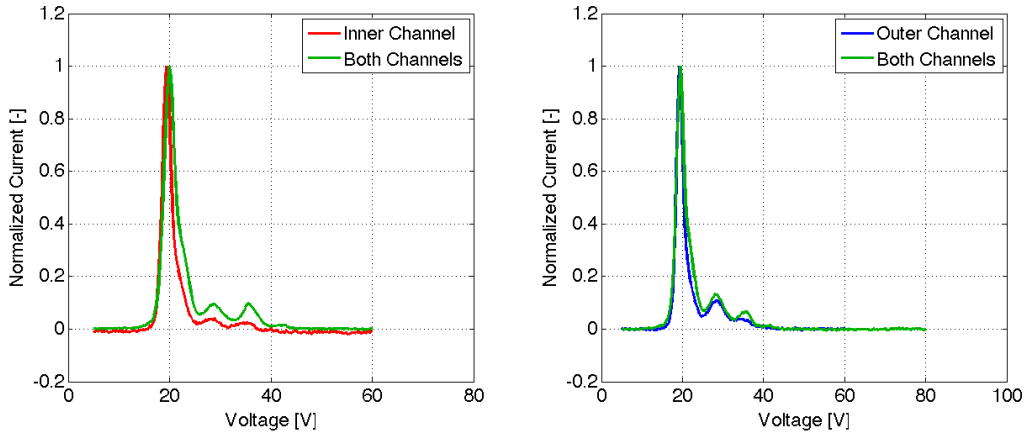

(c) E×B probe spectra at 200V

Figure 11: Single-channel and nested-channel E×B probe spectra at fixed flow rate

Charge utilization efficiencies are shown in Figures 13(a) and 13(b). The calculated values for η_q are typical for Hall thrusters and do not vary significantly with discharge voltage or flow rate. Due to the increase in multiply-charged species in during nested-channel mode, η_Q is typically lower with both channels active, but the drop is still

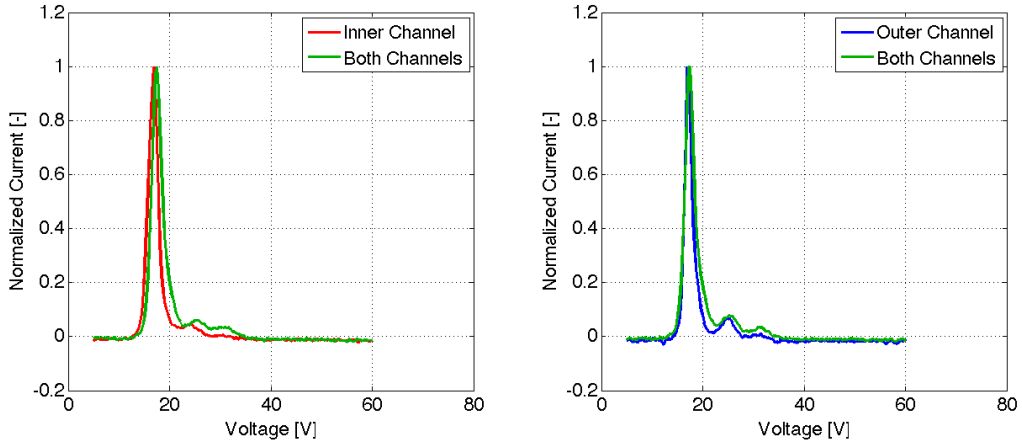

(a) E×B probe spectra at 50% nominal flow rate

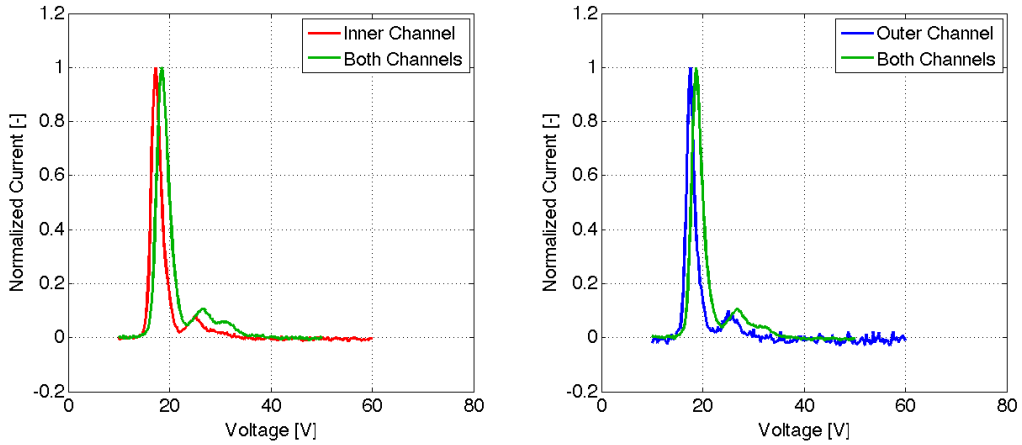

(b) E×B probe spectra at 75% nominal flow rate

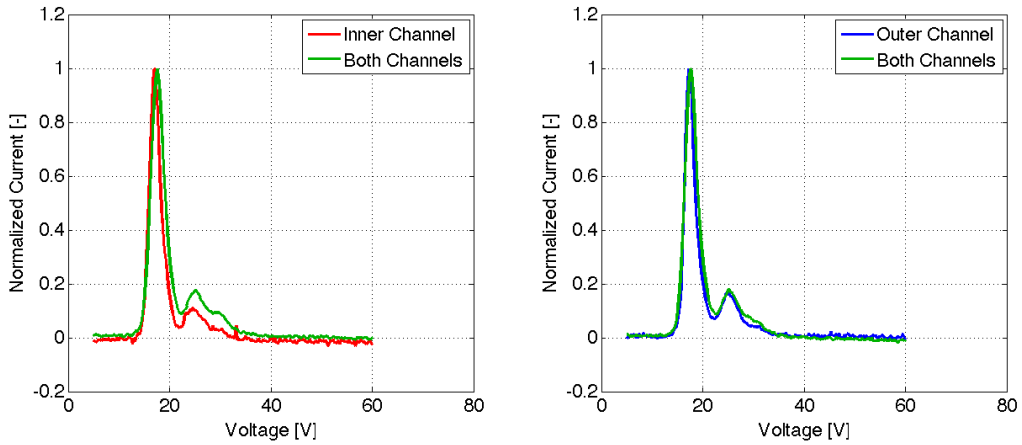

(c) E×B probe spectra at 100% nominal flow rate

Figure 12: Single-channel and nested-channel E×B probe spectra at fixed discharge voltage

small considering the relative values of η_q. Based on prior work with E×B analysis, the relative uncertainty for current fractions is 3% for Ω_1 and 20% for Ω_2 and Ω_3.[9] When necessary, the 20% relative uncertainty was also applied to Ω_4.

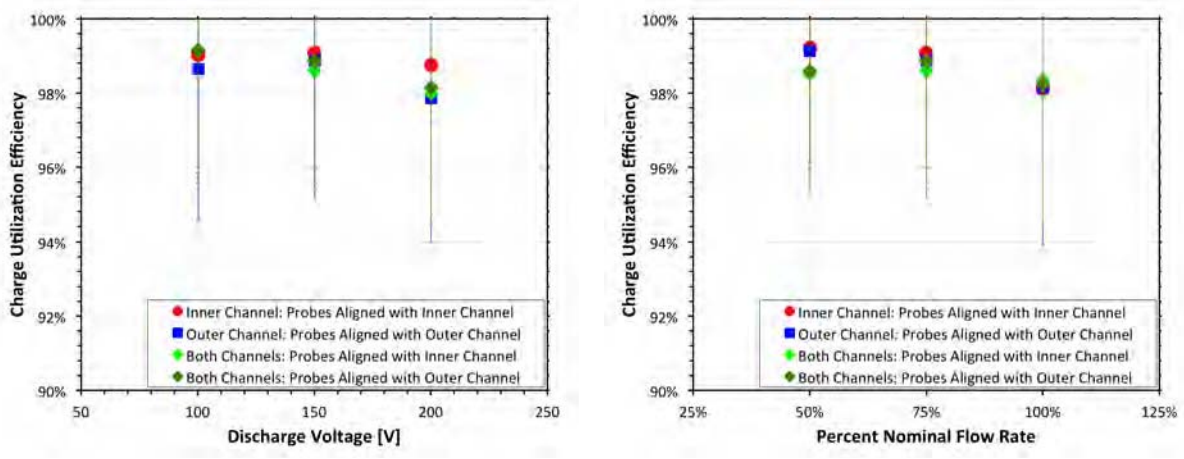

(a) Charge utilization efficiency variation with voltage

(b) Charge utilization efficiency variation with mass flow rate

Figure 13: Charge utilization efficiencies

Mass utilization efficiencies, as based on Faraday probe and E×B probe measurements, are shown in Figures 14(a) and 14(b). Generally, η_m increased with both discharge voltage and flow rate. Differences in η_m between the two operating modes do not appear to be very significant, especially when the compounded measurement error is considered. To improve the uncertainty in η_m, improved measurements of I_b would be necessary.

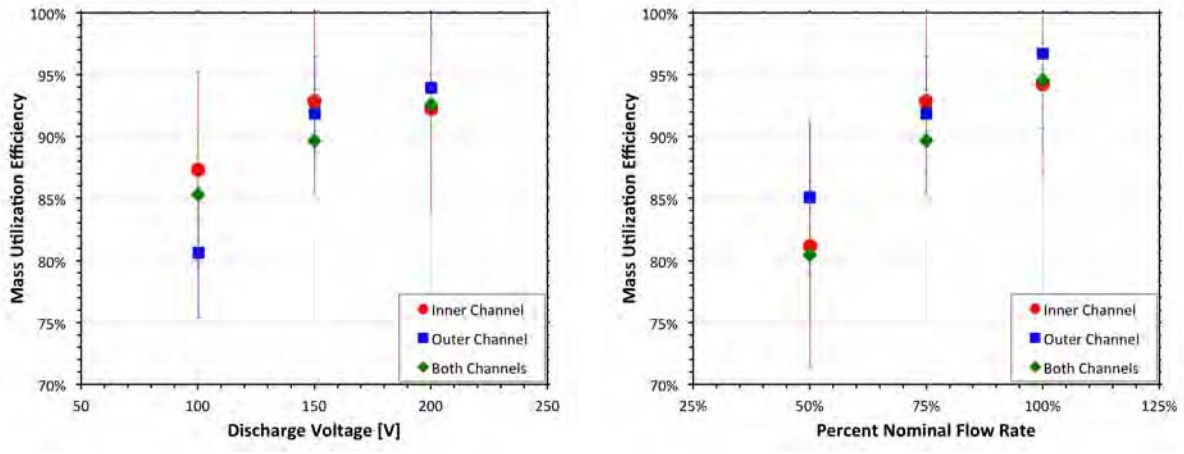

(a) Mass utilization efficiency variation with voltage

(b) Mass utilization efficiency variation with mass flow rate

Figure 14: Mass utilization efficiencies

C. RPA

Figures 15(a) to 16(c) show all RPA traces after processing in order to better indicate the calculated acceleration voltage. The collected currents were numerically differentiated with respect to the voltage of ion retarding grid, and the differentiated signal was subsequently smoothed to remove noise. Using the plasma potential measured by the adjacent Langmuir probe, the differentiated RPA signal was shifted such that the peak was located at V_a. The RPA and Langmuir probe were actuated in the same manner as the E×B, so all plots of RPA traces show measurement taken in alignment with either the inner-channel centerline or outer-channel centerline.

The measured acceleration voltages predictably increased with discharge voltage and remained relatively insensitive to flow rate. Unexpectedly, the differences in measured values of V_a between operating modes show comparable

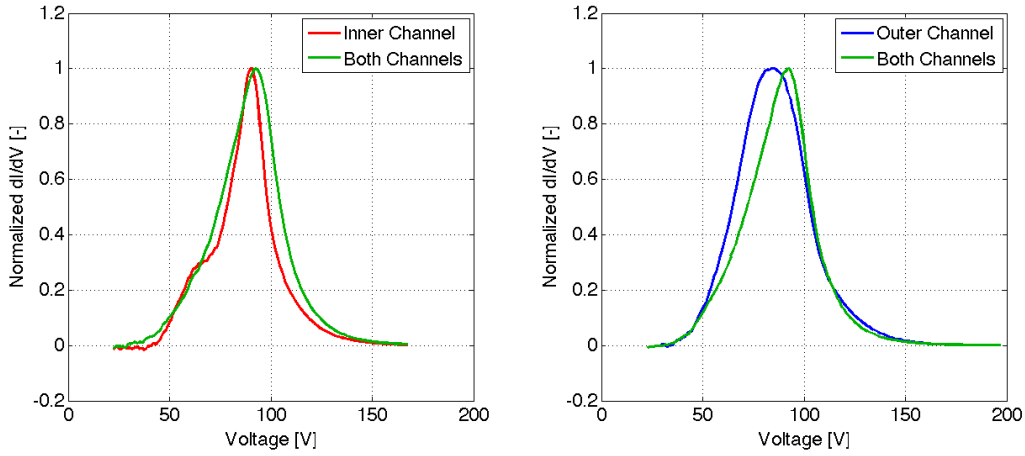

(a) Corrected and differentiated RPA traces at 100V

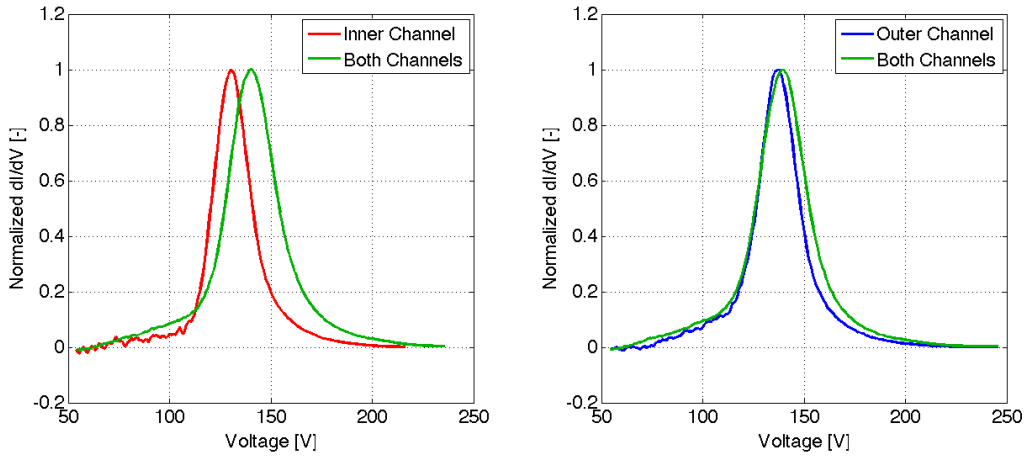

(b) Corrected and differentiated RPA traces at 150V

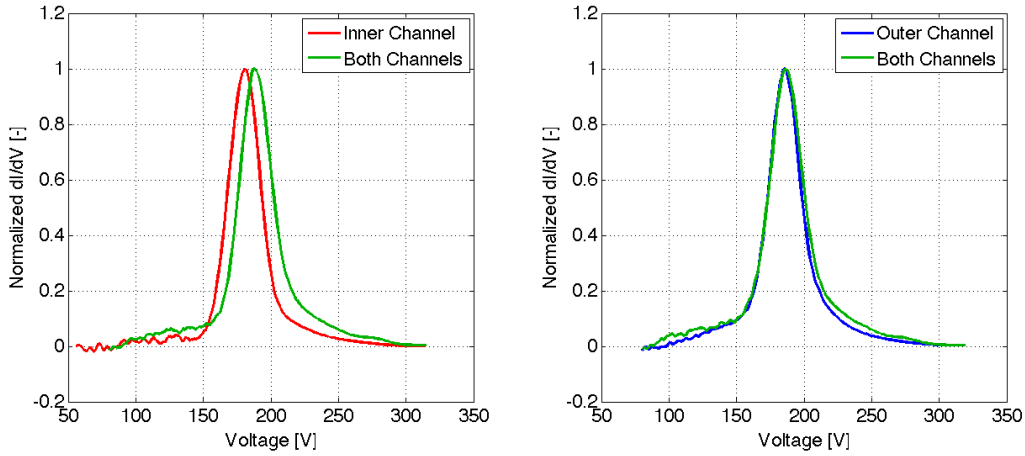

(c) Corrected and differentiated RPA traces at 200V

Figure 15: Single-channel and nested-channel corrected and differentiated RPA traces at fixed flow rate

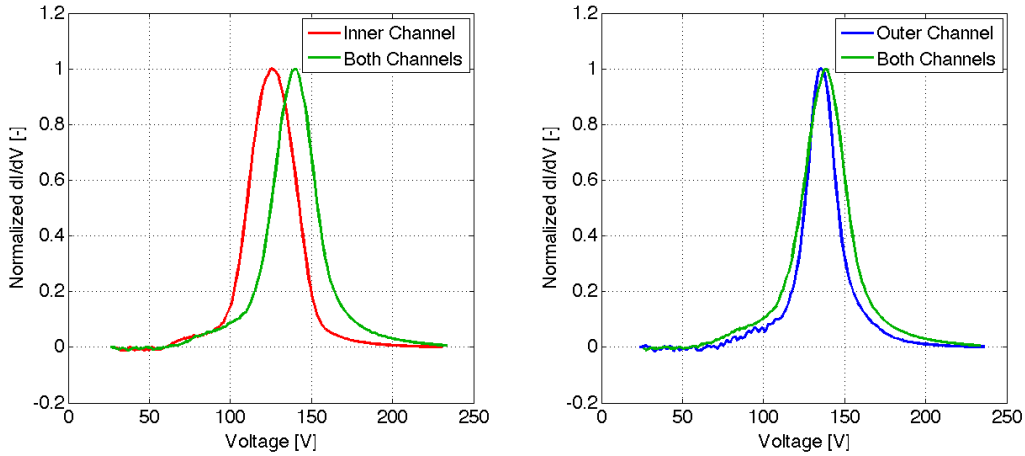

(a) Corrected and differentiated RPA traces at 50% nominal flow rate

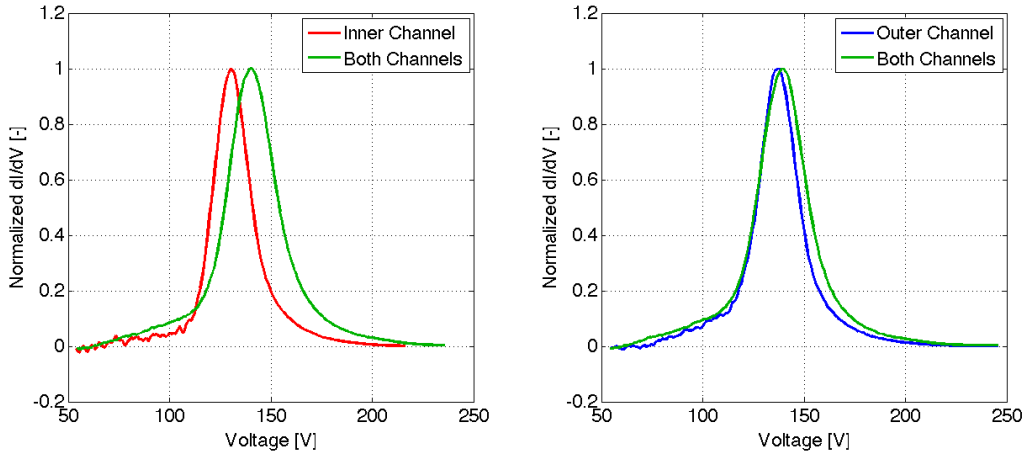

(b) Corrected and differentiated RPA traces at 75% nominal flow rate

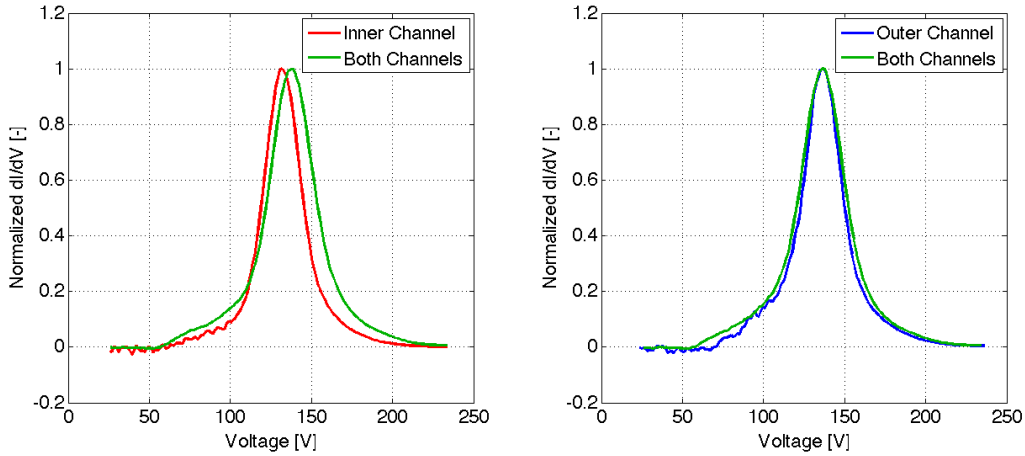

(c) Corrected and differentiated RPA traces at 100% nominal flow rate

Figure 16: Single-channel and nested-channel corrected and differentiated RPA traces at fixed discharge voltage

or higher acceleration with both channels active. The higher V_a was particularly pronounced for the inner channel at the operating point of interest: 150V and 75% nominal flow rate. For the majority of operating conditions, the difference in V_a for the outer channel was relatively small.

The trends in voltage utilization, as shown in Figures 17(a) and 17(b), reflect the trends in V_a. η_v increases with discharge voltage, remains relatively constant with flow rate, and increases with both channels active. The increase in η_v is greatest between the inner-channel and nested-channel operating conditions except at 100 V. Uncertainty in η_v is dominated by the uncertainty in acceleration voltage and in plasma potential. Based on the uncertainty of the numerical methods and signal noise, the estimated uncertainty for V_a ranged from 3 V to 5 V and the uncertainty for V_p was approximately 2 V. The uncertainty in V_d is estimated at ±0.25 V.

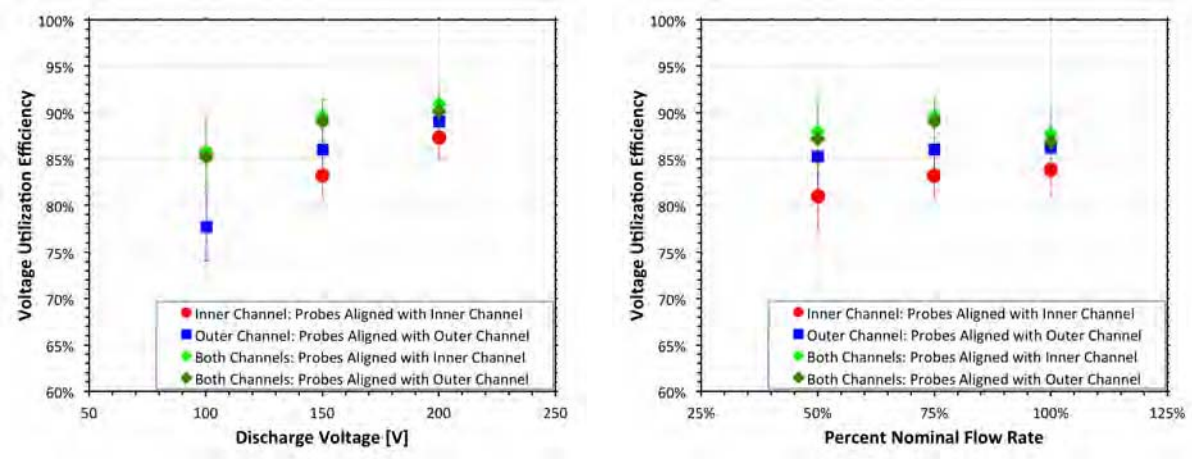

(a) Voltage utilization efficiency variation with voltage

(b) Voltage utilization efficiency variation with mass flow rate

Figure 17: Voltage utilization efficiencies

V. Discussion

The results of the far-field diagnostics show that the X2 NHT behaves in a similar manner as a typical Hall thruster in the low-voltage, high thrust-to-power operating regime. The far-field Faraday probe measurements yield typical low-voltage current density profiles, and the E×B and RPA measurements by themselves do not yield anything unique when both channels are at the same discharge voltage. The values for all utilization efficiencies are within expected ranges, and the trends with respect to discharge voltage and flow rate are typical as well.

The comparison between measured total efficiencies and calculated total efficiencies based on the existing models are shown in Figures 18(a) and 18(b). The absolute difference between the measured and calculated total efficiencies vary from 1% to 6%. Given the small difference, the results of the far-field measurements also show that existing efficiency models can be applied to an NHT with only minor modifications to Faraday probe analysis.

The small gains in performance from the X2's nested-channel operation, as illustrated in Figure 2, are most likely due to the increased voltage utilization, and this phenomenon appears in the measurements of most of the probes employed in this study. The higher acceleration voltages in nested-channel mode resulted in shifts in E×B measurements, as seen previously in all E×B spectra. Additionally, cathode coupling voltages were calculated using the far-field Langmuir probe measurements and are shown in Figures 19(a) and 19(b). The cathode-coupling voltages are consistently lower in the nested-channel mode, implying that more of the discharge voltage is used to accelerate ions.

The increase in voltage utilization is one of the few unique features of the nested-channel mode, and its occurrence shows that the two channels can interact in an advantageous manner. However, at present, the gains are relatively small but may be exploitable with further study.

VI. Conclusion

Far-field plume measurements were performed on the X2 nested-channel Hall thruster using an array of diagnostics in order to study how the individual channels combine during simultaneous operation. The diagnostics utilized during

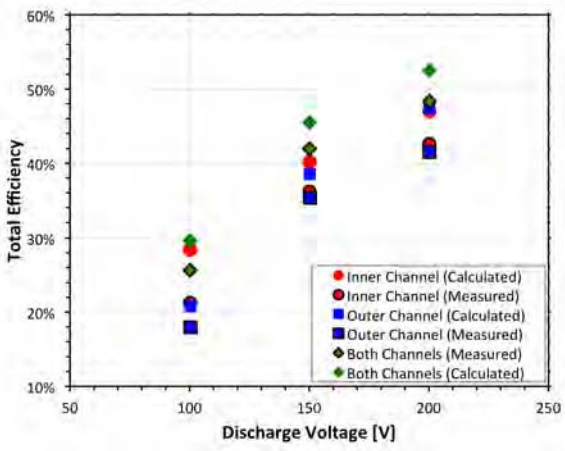

(a) Variation of total efficiencies with discharge voltage

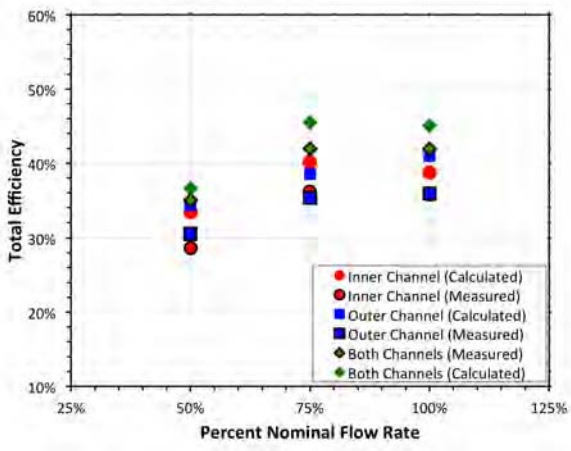

(b) Variation of total efficiencies with mass flow rate

Figure 18: Total efficiencies

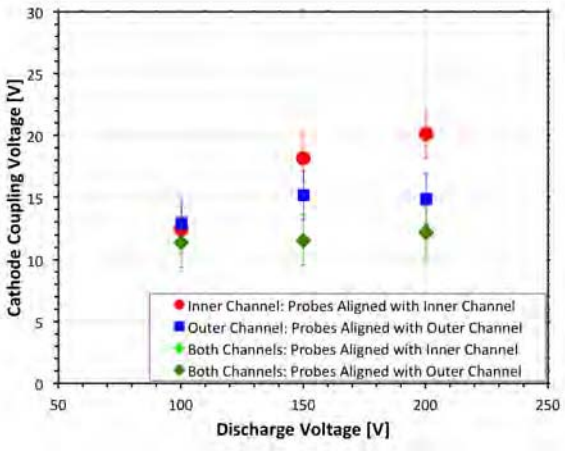

(a) Variation of cathode coupling voltage with discharge voltage

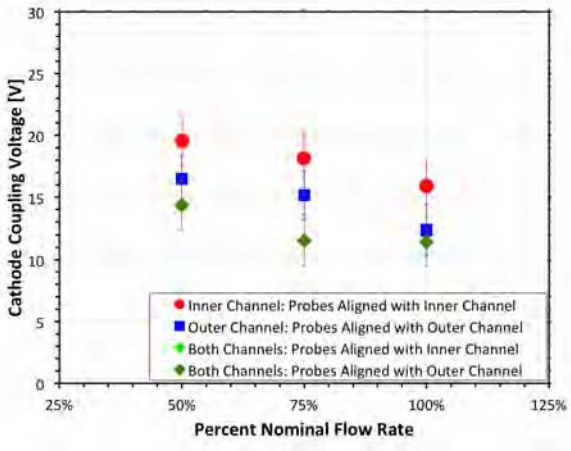

(b) Variation of cathode coupling voltage with mass flow rate

Figure 19: Cathode coupling voltages

this study include a nude Faraday probe, retarding potential analyzer, and E×B probe. Data from these probes were used to calculate the following utilization efficiencies that contribute to the total efficiency of the thruster:

- Current utilization efficiency, η_b
- Divergence efficiency, η_d
- Charge utilization efficiency, η_q
- Voltage utilization efficiency, η_v
- Mass utilization efficiency, η_m

Comparisons of utilization efficiencies during nested-channel against those of single-channel operation show an increase in voltage utilization and a slight decrease in charge utilization. The increase in voltage utilization consistently corresponded to a decrease in cathode-coupling voltage. Mass utilization, current utilization, and beam divergence remained near the values measured during operation of individual channels.

A nested-channel Hall effect thruster has been shown to operate much like a conventional Hall thruster when all available channels are at the same discharge voltage. Far-field diagnostics have been able to resolve small differences between the two channels. One unique feature of the NHT is the improved ion acceleration with both channels active. Subsequent investigation will possibly focus on the internal and very-near-field plasma potential distribution of the X2 in order to gain further understanding of this phenomenon.

Acknowledgements

The authors would like to thank our sponsors at the Air Force Research Laboratory, including Dr. Daniel Brown, Dr. Brian Beal, and Dr. James Haas. Additional insight regarding Faraday probes, low-voltage Hall thruster operation, and efficiency analysis from Dr. Brown was greatly appreciated. We would also like to thank the AFRL for the new LaB_6 cathode and RPA used in our experiments. Thanks go to Rohit Shastry, Roland Florenz, Adam Shabshelowitz, Käthe Dannenmayer du Centre National de la Recherche Scientifique, and Cameron Lee of Cornell University for their assistance with the experiments performed for this study. Raymond Liang is supported by the National Defense Science and Engineering Graduate (NDSEG) Fellowship.

Appendix: Mixed-Voltage Operation

The majority of the operating conditions used during testing of the X2 match the discharge voltages and current densities between the two channels. However, operation with mixed discharge voltages has been investigated with a small number of additional conditions. No mixed-voltage condition has yielded a particularly unique performance advantage, and, in most cases, these operating modes have comparable performance to matched-voltage conditions. However, measurements from a far-field RPA and E×B have produced some unique spectra.

This appendix shows the results of RPA and E×B measurements for the flow rate combination of 7.0 mg/s through the inner channel and 17.4 mg/s through the outer channel. The discharge voltage applied to the inner was fixed at 150 V, and the outer channel discharge voltage was increased to 200 V and 300 V. The cathode flow fraction was fixed at 10%, and the electromagnets were tuned to maximize efficiency at each operating condition.

Figure 20 shows processed RPA measurements which include smoothing of the differentiated signal and voltage correction for local plasma potential. The sweeps shown in Figure 20 were taken with the RPA aligned with the outer channel centerline. Measurements during the mixed-voltage conditions how bimodal distributions with peaks near the two applied discharge voltages. At a distance of 2.1 m, the RPA clearly collects ions from both channels. Current collected from the inner channel has a weaker signal due to the lower total current of the inner channel and the probe's alignment. However, both peaks remain well-defined and the two acceleration voltages can be measured from RPA traces taken during a single mixed-voltage condition.

Figure 21 shows the evolution of the E×B spectra as the outer discharge voltage is increased to 300V. The dominant peaks in the spectra shift to higher voltages, as expected. A smaller peak is present at a voltage lower than the dominant peak. As shown in Figure 22, this smaller peak corresponds to the singly-charged ion population from the inner channel. Having fallen through a smaller potential drop, the inner channel ions register as a small population of slower ions.

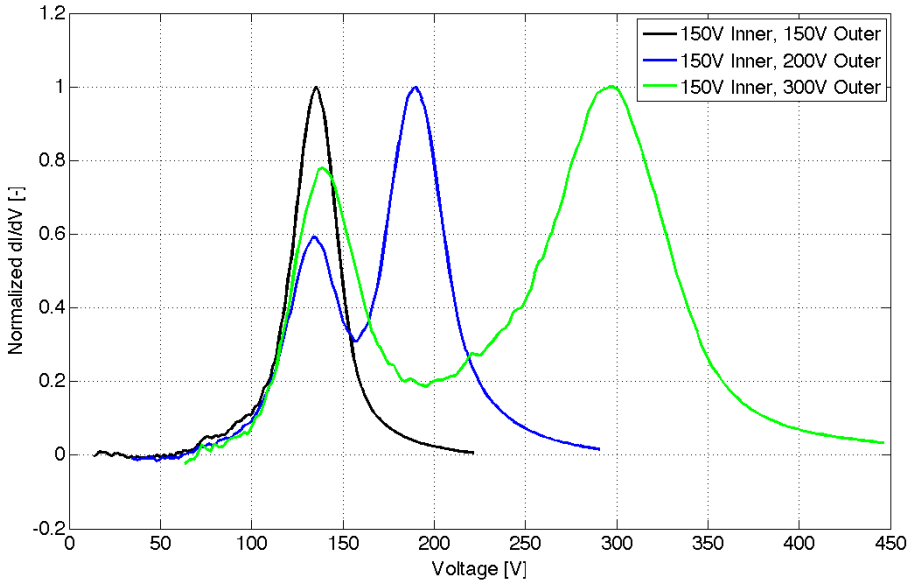

Figure 20: RPA measurements for mixed-voltage operating conditions

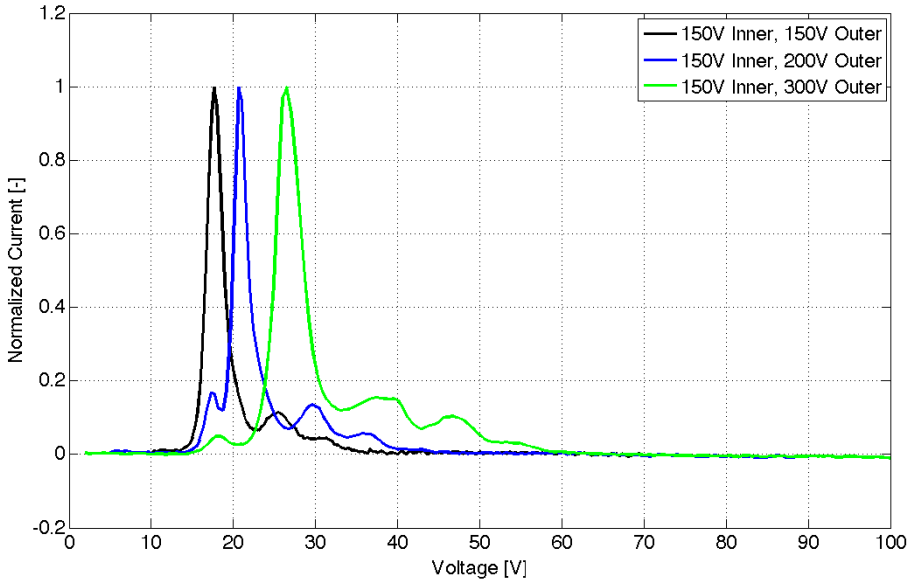

Figure 21: E×B measurements for mixed-voltage operating conditions

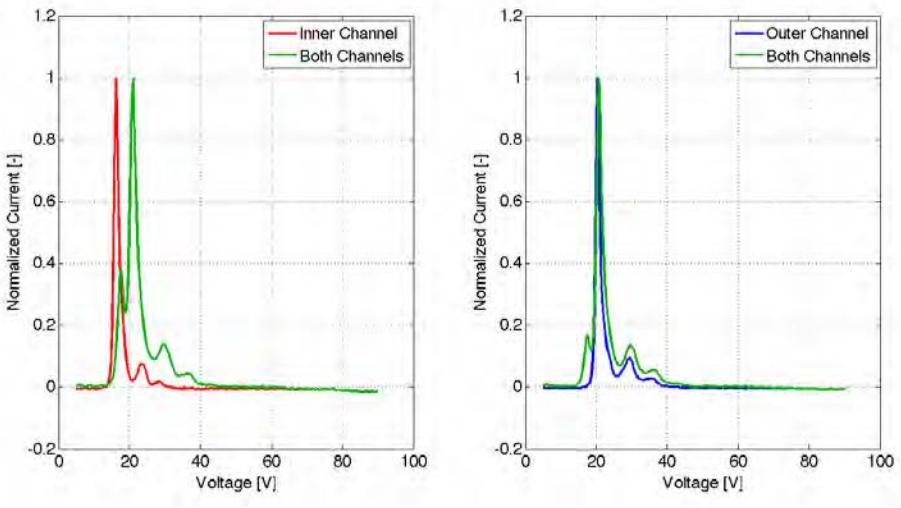

Figure 22: Single-channel and nested-channel E×B measurements for a mixed-voltage operating condition (150V inner channel, 200 V outer channel, 7.0+17.4 mg/s)

Figure 22 also shows that multiply-charged species from the inner channel are not resolved in the nested-channel spectrum, and therefore, quantifying species fractions becomes slightly more involved during mixed-voltage operating conditions. The inner-channel signal is obscured by the higher signal provided by the outer channel, and in order to determine the multiply-charge species fractions of the inner channel, single-channel measurements had to be taken. However, it is possible that, if the discharge voltage difference were sufficiently large between the two channels, all multiply-charged peaks from both channels would appear on an E×B spectrum. This would require the singly-charged ions from the outer channel to move faster than the triply-charged or quadruply-charged ions from the inner channel.

References

[1]Jacobson, D.T., John, J.W., Kamhawi, H., Manzella, D.H, and Peterson, P.Y., "An Overview of Hall Thruster Development at NASA's John H. Glenn Research Center," *AIAA/ASME/SAE/ASEE Joint Propulsion Conference and Exhibit*, Tucson, AZ, July 2005, pp. 1–15.

[2]Spores, R., Monheiser, J., Dempsey, B.P., Wade, D., Creel, K., Jacobson, D., and Drummond, G., "A Solar Electric Propulsion Caro Vehicle to Support NASA Lunar Exploration Program," *International Electric Propulsion Conference*, Princeton, NJ, October 2005, pp. 1–22.

[3]Wilson, F., "Propulsion and Energy: Electric Propulsion," *Aerospace America*, December 2006.

[4]Brown, D.L., Beal, B.E., and Haas, J.M., "Air Force Research Laboratory High Power Electric Propulsion Technology Development," *IEEE Aerospace Conference*, Big Sky, MT, March 2010, pp. 1–9.

[5]Hofer, R.R., Katz, I., Mikellides, I.G., Goebel, D.M., Jameson, K.K., Sullivan, R.M., and Johnson, L.K, "Efficacy of Electron Mobility Models in Hybrid-PIC Hall Thruster Simulations," *AIAA/ASME/SAE/ASEE Joint Propulsion Conference and Exhibit*, Hartford, CT, July 2008, pp. 1–29.

[6]Brown, D.L., Larson, C.W., Beal, B.E., and Gallimore, A.D., "Methodology and Historical Perspective of a Hall Thruster Efficiency Analysis," *Journal of Propulsion and Power*, Vol. 25, No. 6, 2009, pp. 1163–1177.

[7]Brown, D.L. and Gallimore, A.D., "Evaluation of Ion Collection Area in Faraday Probes," *Review of Scientific Instruments*, Vol. 81, No. 063504, 2010, pp. 1–11.

[8]Brown, D.L. and Gallimore, A.D., "Faraday Probe Analysis, Part 2: Evaluation of Facility Effects on Ion Migration in a Hall Thruster Plume," Preprint.

[9]Shastry, R., Hofer, R.R., Reid, B.M, and Gallimore, A.D., "Method for Analyzing E×B Probe Spectra from Hall Thruster Plumes," *Review of Scientific Instruments*, Vol. 80, No. 063502, 2009, pp. 1–11.

[10]Hofer, R.R., *Development and Characterization of High-Efficiency, High-Specific Impulse Xenon Hall Thrusters*, Ph.D. thesis, University of Michigan, Ann Arbor, MI, 2004.

[11]Beal, B.E., *Clustering of Hall Effect Thrusters for High-Power Electric Propulsion Applications*, Ph.D. thesis, University of Michigan, Ann Arbor, MI, 2005.

[12]Walker, M.L.R. and Gallimore, A.D., "Performance Characteristics of a Cluster of 5-kW Laboratory Hall Thrusters," *Journal of Propulsion and Power*, Vol. 23, No. 1, 2007, pp. 35–43.

[13]Reid, B.M., Shastry, R., Gallimore, A.D., and Hofer, R.R., "Angulary-Resolved E×B Probe Spectra in the Plume of a 6-kW Hall Thruster," *AIAA/ASME/SAE/ASEE Joint Propulsion Conference and Exhibit*, Hartford, CT, July 2008, pp. 1–21.

[14]Reid, B.M., *The Influence of Neutral Flow Rate in the Operation of Hall Thrusters*, Ph.D. thesis, University of Michigan, Ann Arbor, MI, 2009.

[15]Varian, "Vacuum Measurement Catalog," 2010.

[16]Brown, D.L., *Investigation of Low Discharge Voltage Hall Thruster Characteristics and Evaluation of Loss Mechanisms*, Ph.D. thesis, University of Michigan, Ann Arbor, MI, 2009.

Far-Field Plume Measurements of a Nested-Channel Hall-Effect Thruster

R. Liang and A.D. Gallimore

Plasmadynamics and Electric Propulsion Laboratory

University of Michigan

UNIVERSITY OF MICHIGAN

Presentation Overview

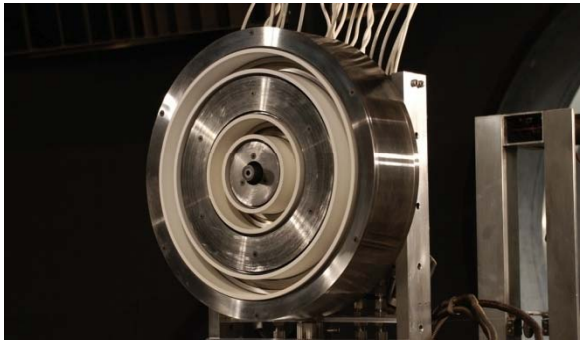

Introduction to the X2

Far-Field Plume Measurements

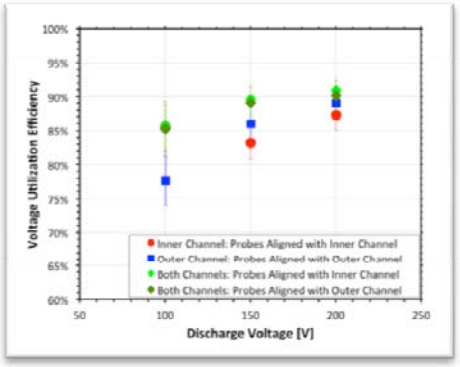

Utilization Efficiencies

Introduction

- X2 was developed to explore the capabilities and to verify the advantages of nested-channel Hall thrusters
- Both channels are designed to be comparable to each other
- Cross-sectional dimensions of discharge channels are the same
- Anode designs are also identical[5]

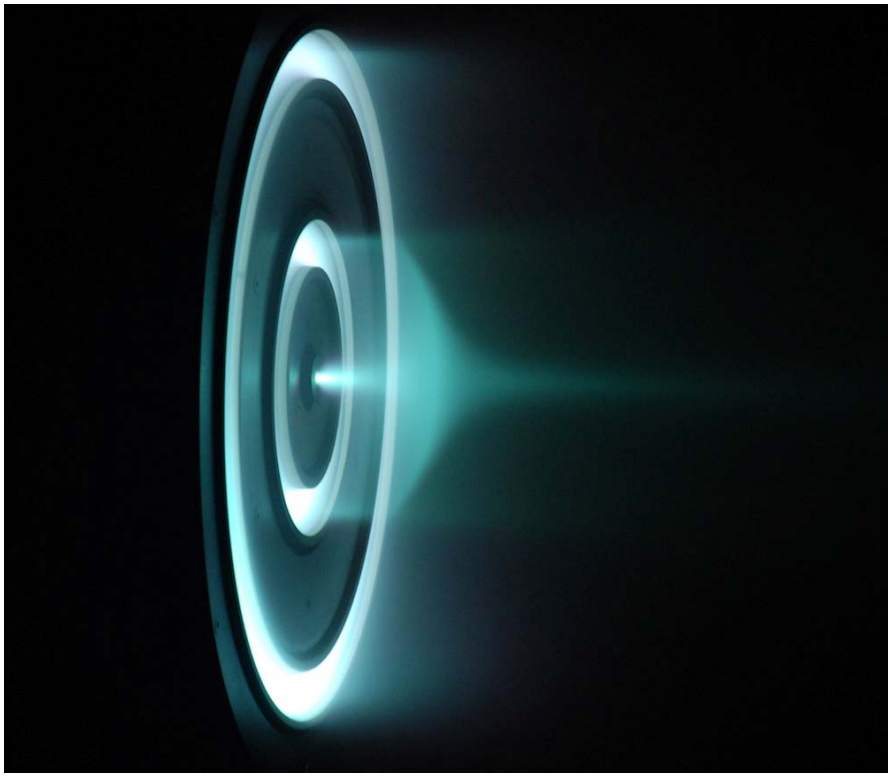

Magnetic Circuit

- Magnetic circuit creates the same magnetic field topology in both channels
- Each channel has two magnets, much like a conventional Hall thruster
- Plasma lens topology used based on past designs from PEPL, AFRL, and NASA
- Radial magnetic field direction switches between channels

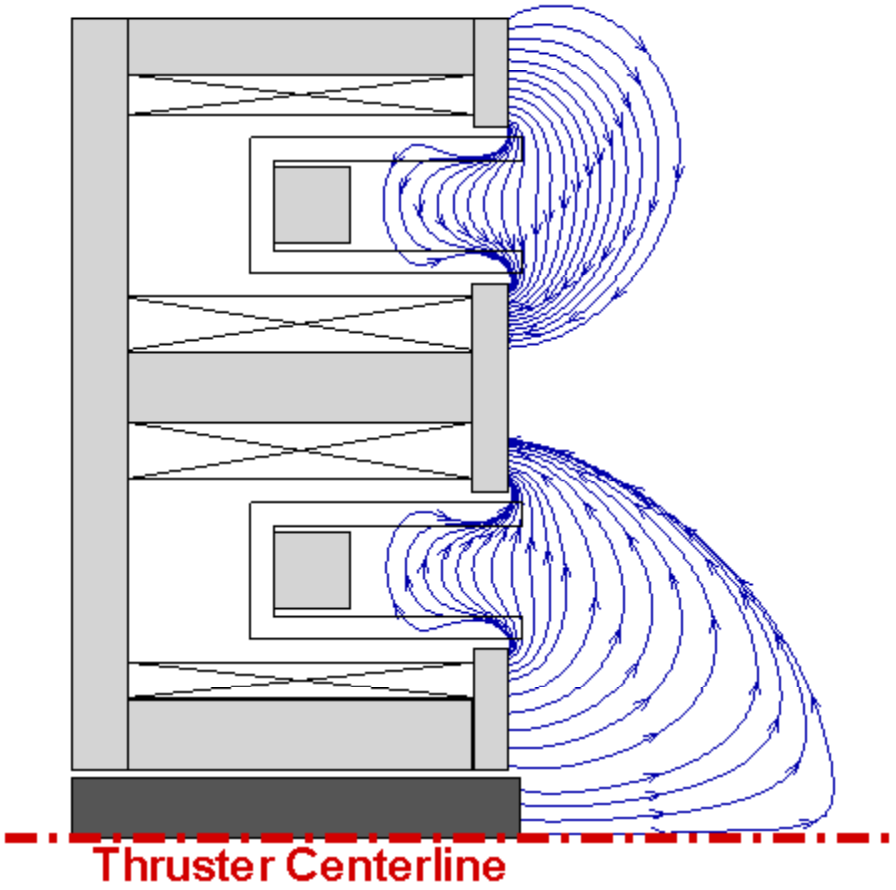

Performance Increase in Nested-Channel Mode

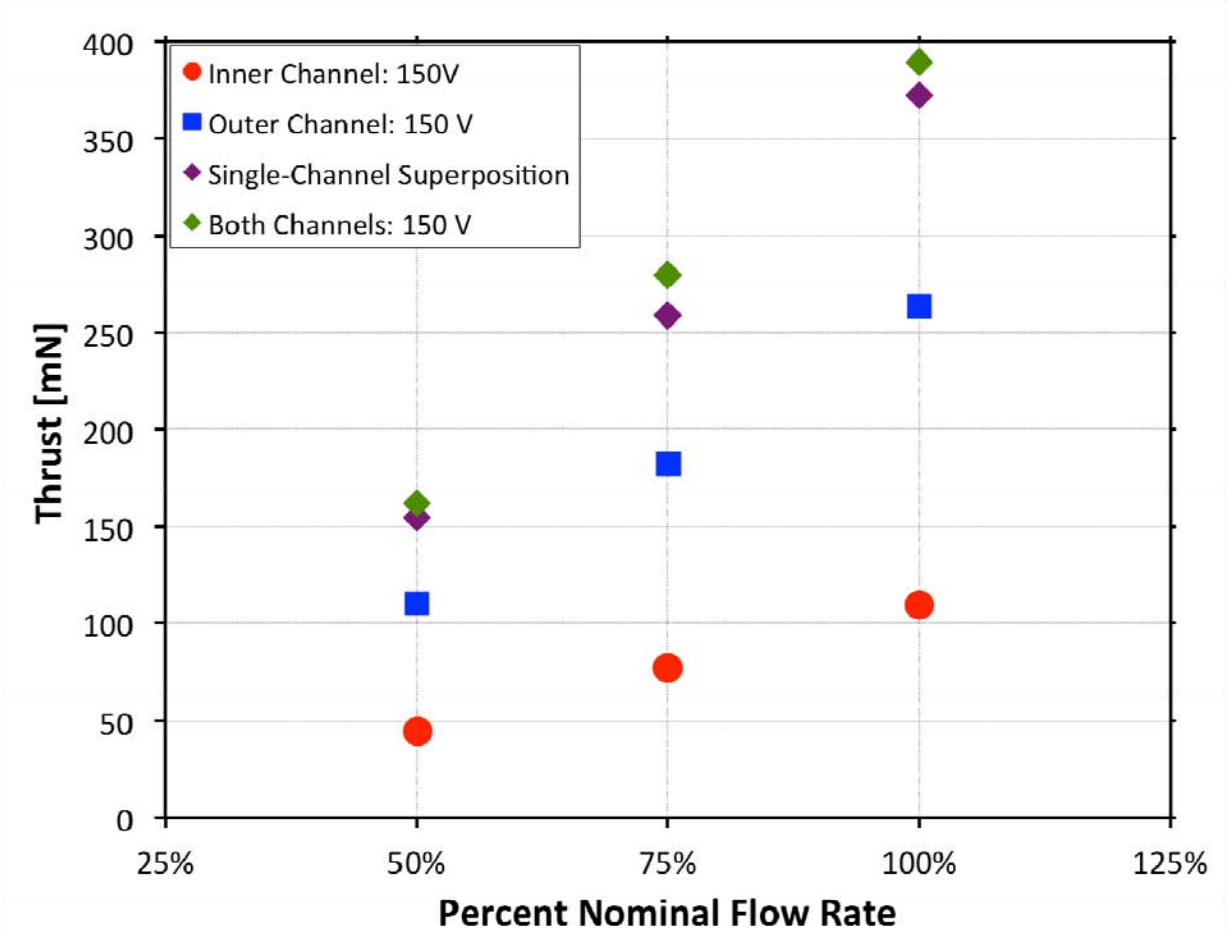

UNIVERSITY OF MICHIGAN

Probes

- Faraday probe
- E×B
- Retarding potential analyzer with Langmuir probe

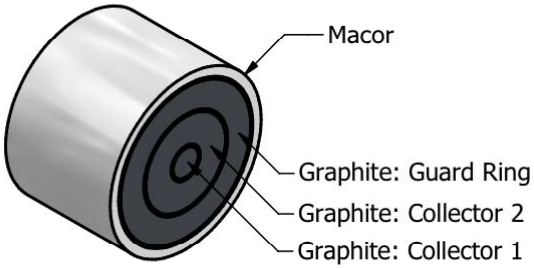

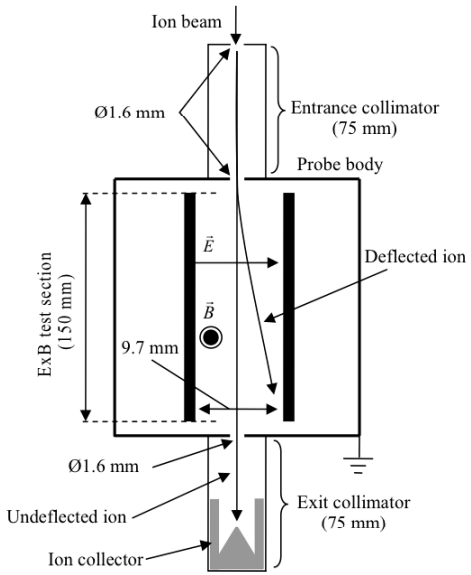

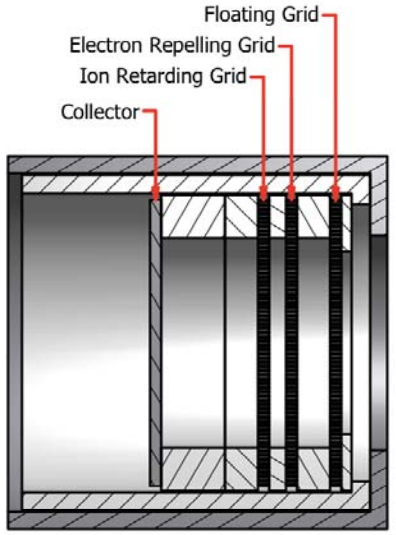

UNIVERSITY OF MICHIGAN

Operating Conditions

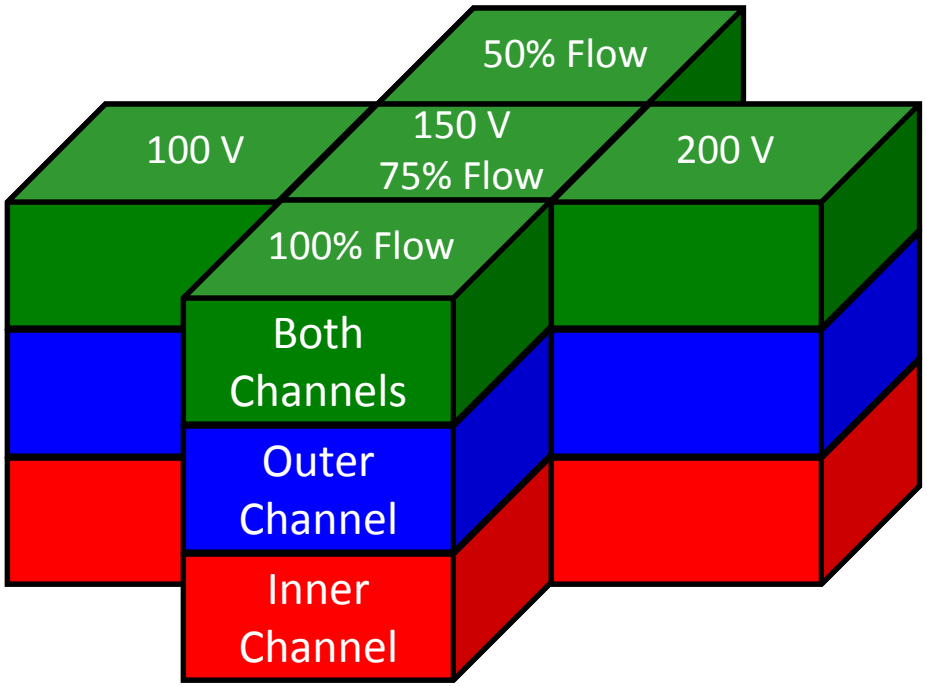

Discharge Voltage [V]	Inner Mass Flow Rate [mg/s]	Outer Mass Flow Rate [mg/s]
100	7.0	17.4
150	4.7	11.6
150	7.0	17.4
150	9.3	23.2
200	7.0	17.4
100	7.0	-
150	4.7	-
150	7.0	-
150	9.3	-
200	7.0	-
100	-	17.4
150	-	11.6
150	-	17.4
150	-	23.2
200	-	17.4

Current Density Profiles at Constant Flow Rate

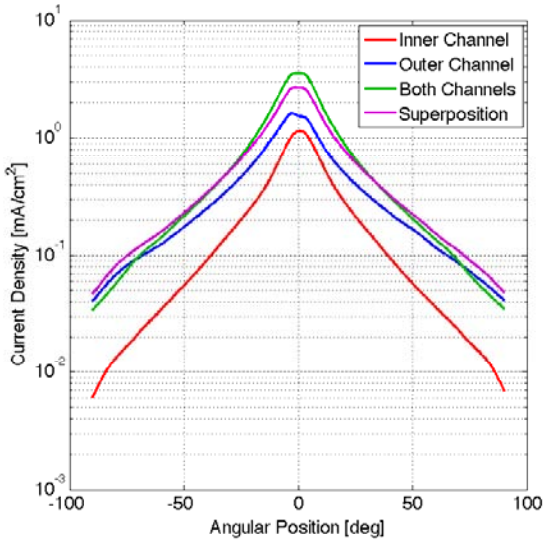

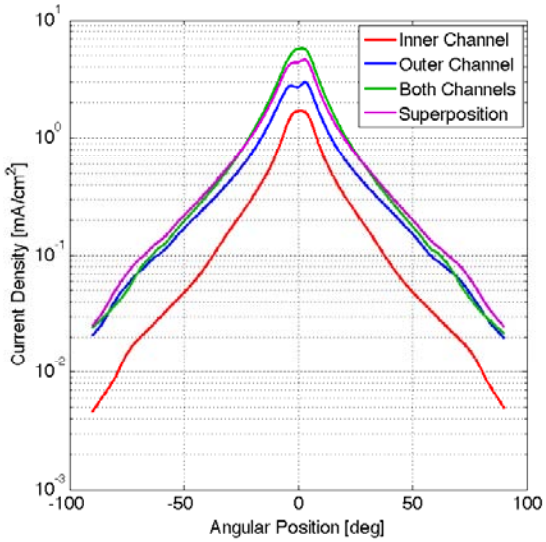

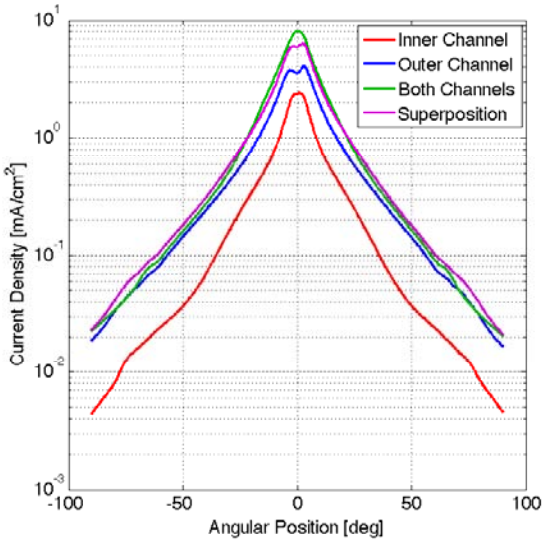

Current Density Profiles at Constant Discharge Voltage

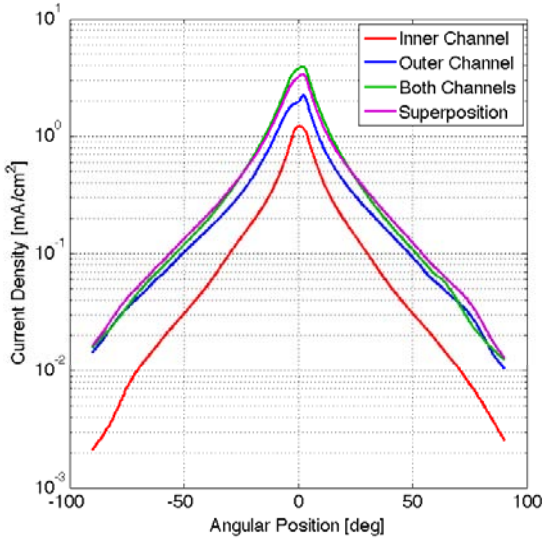

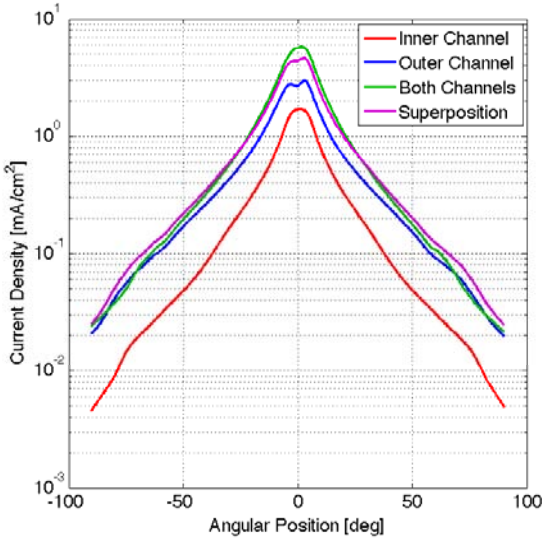

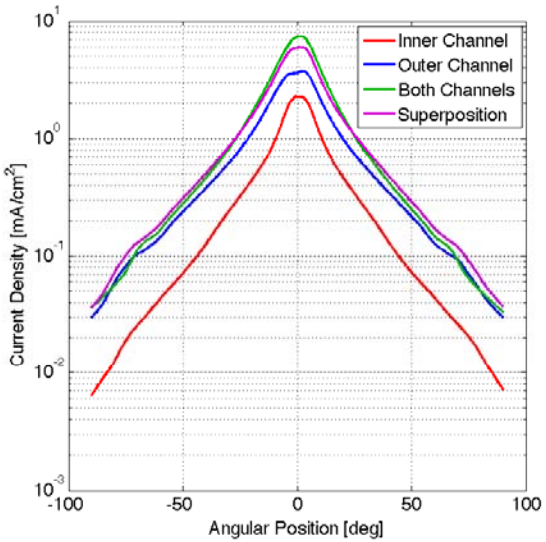

E×B Spectra at Constant Flow Rate

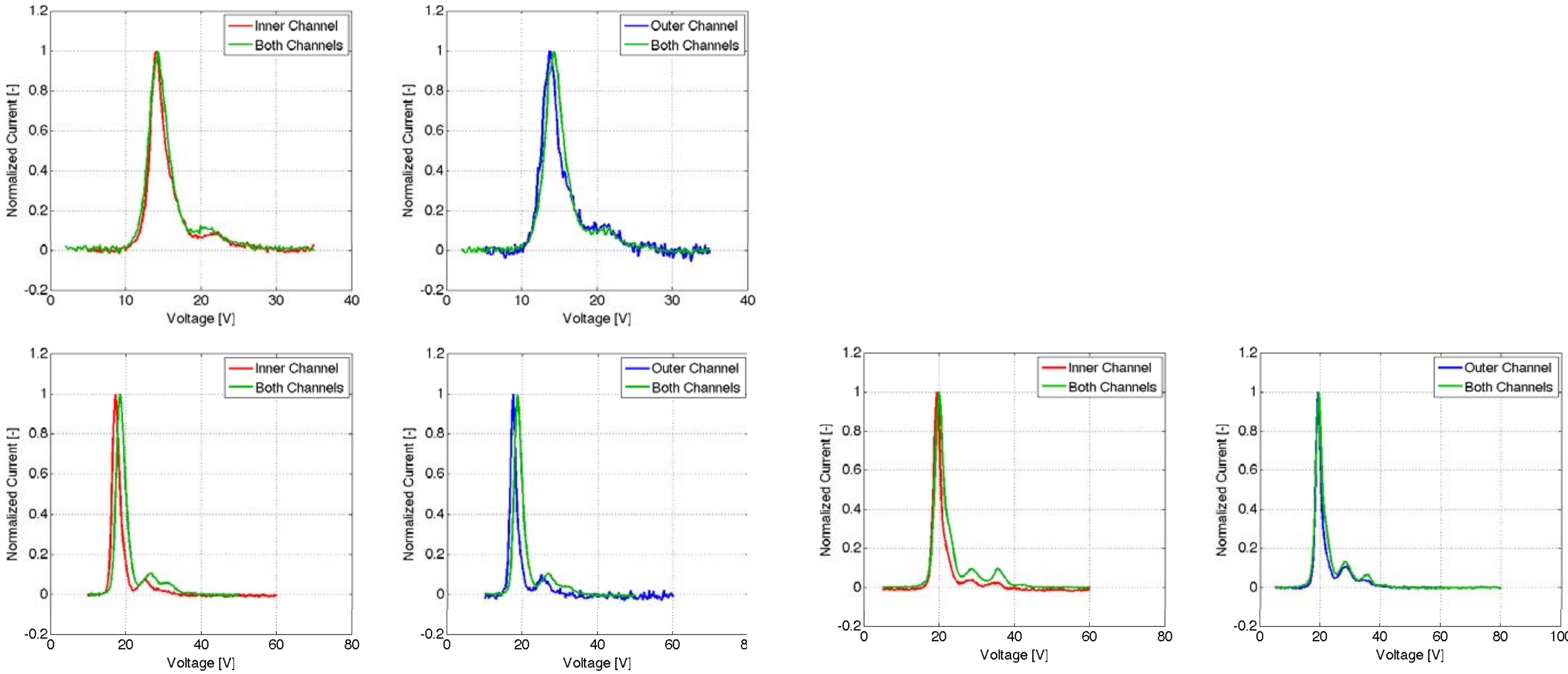

Distribution Statement A. Approved for public release; distribution is unlimited.

E×B Spectra at Constant Discharge Voltage

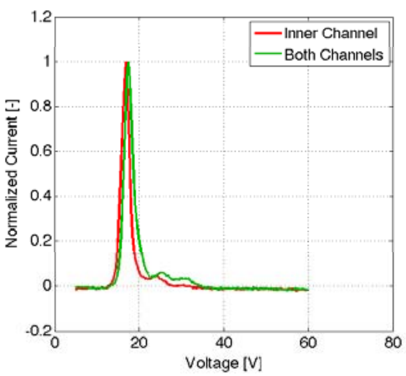

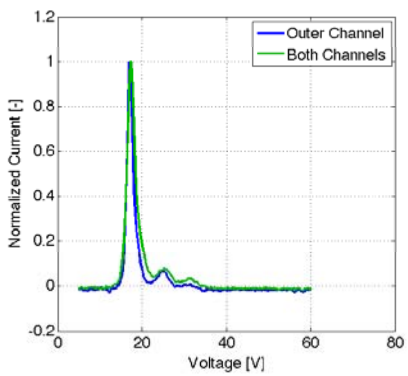

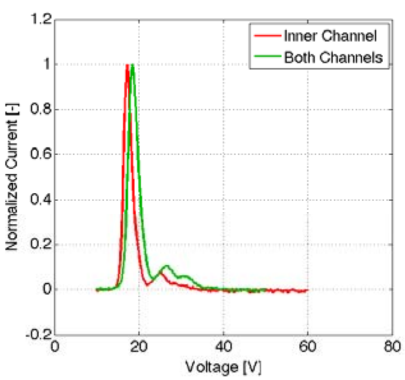

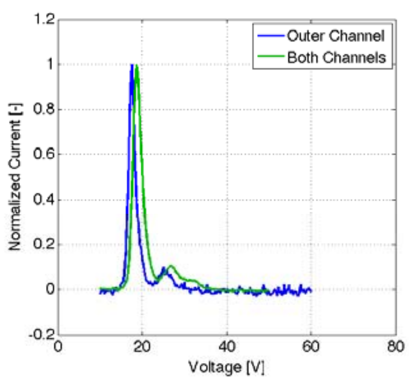

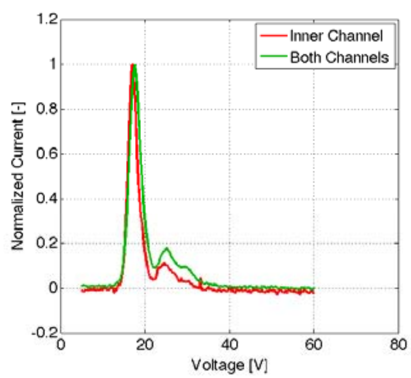

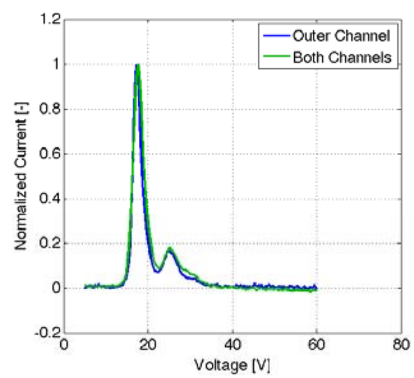

RPA Measurements at Constant Flow Rate

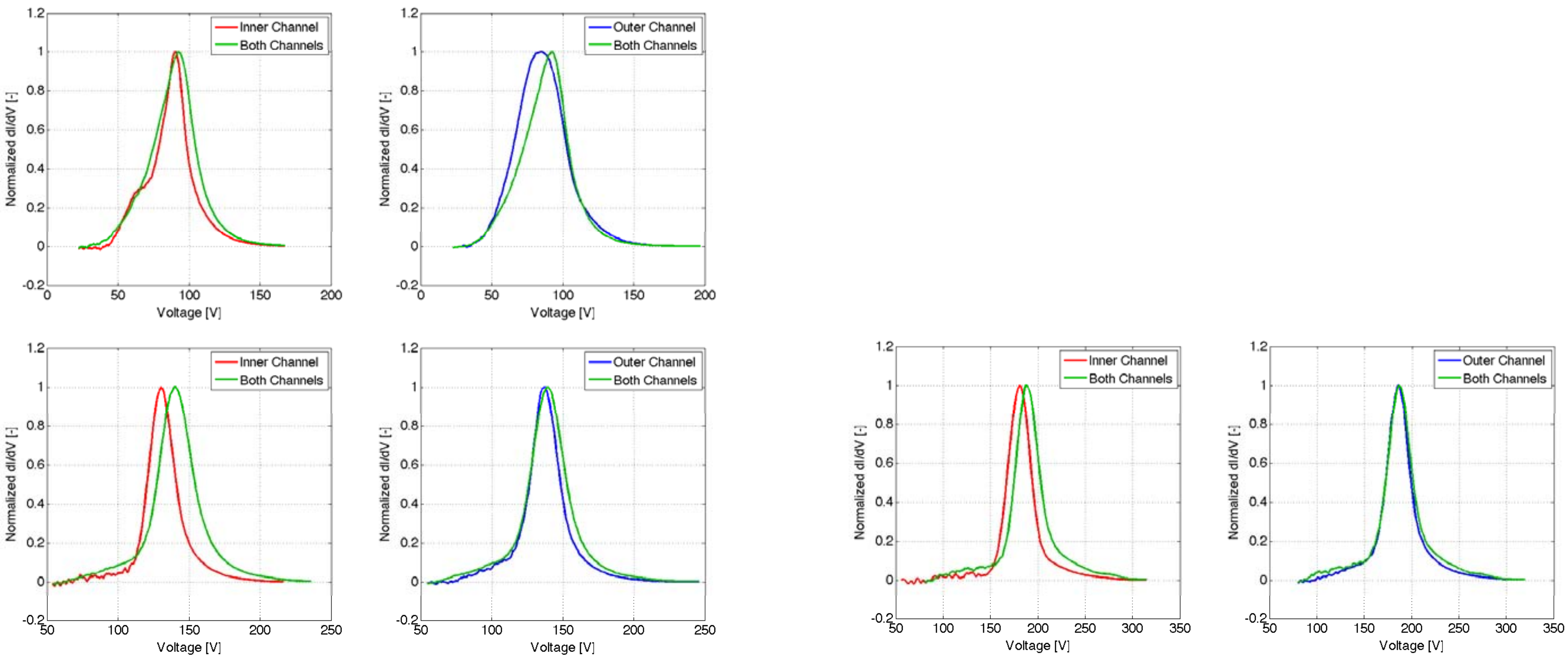

RPA Measurements at Constant Discharge Voltage

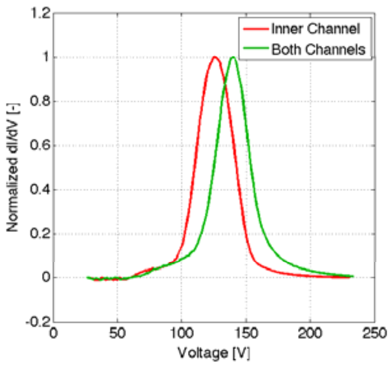

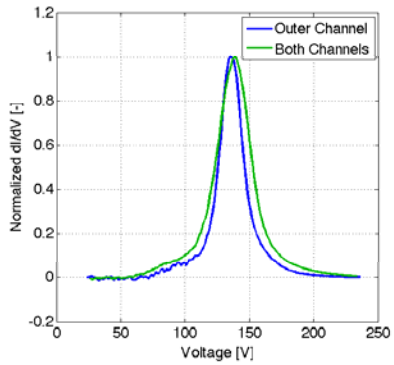

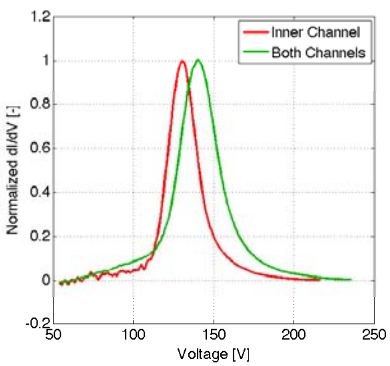

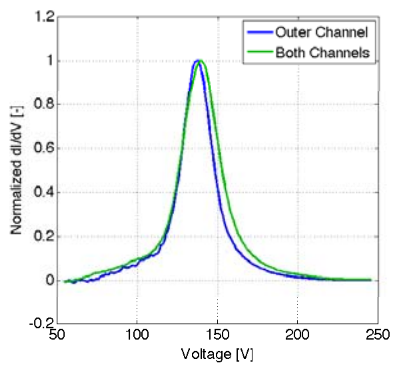

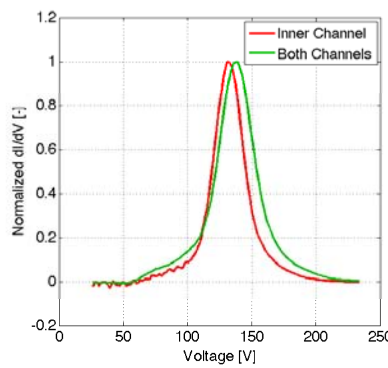

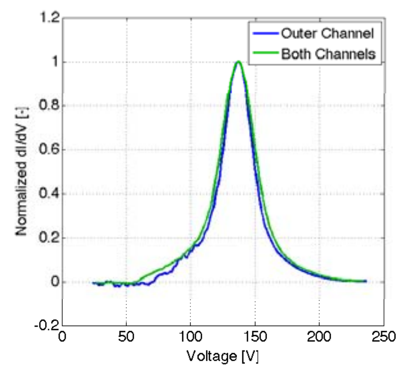

Current Utilization Efficiencies

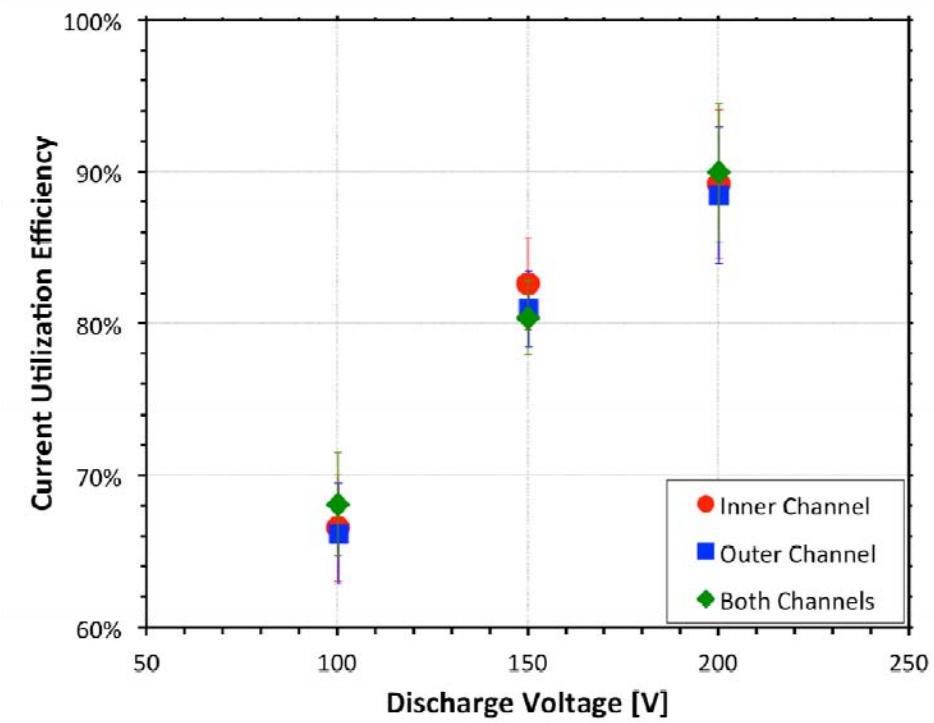

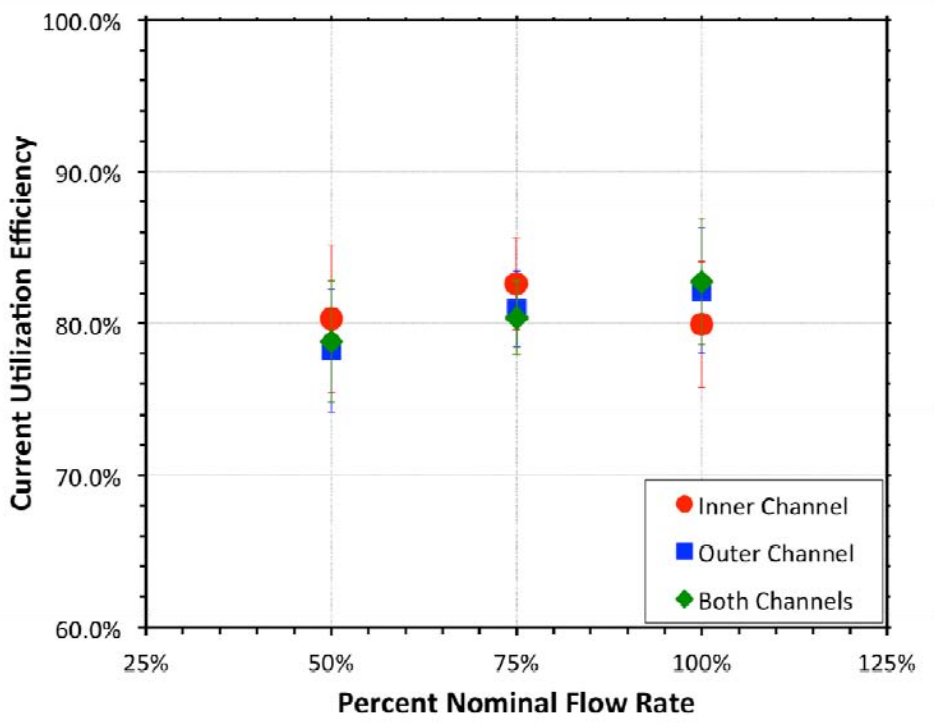

Divergence Efficiencies

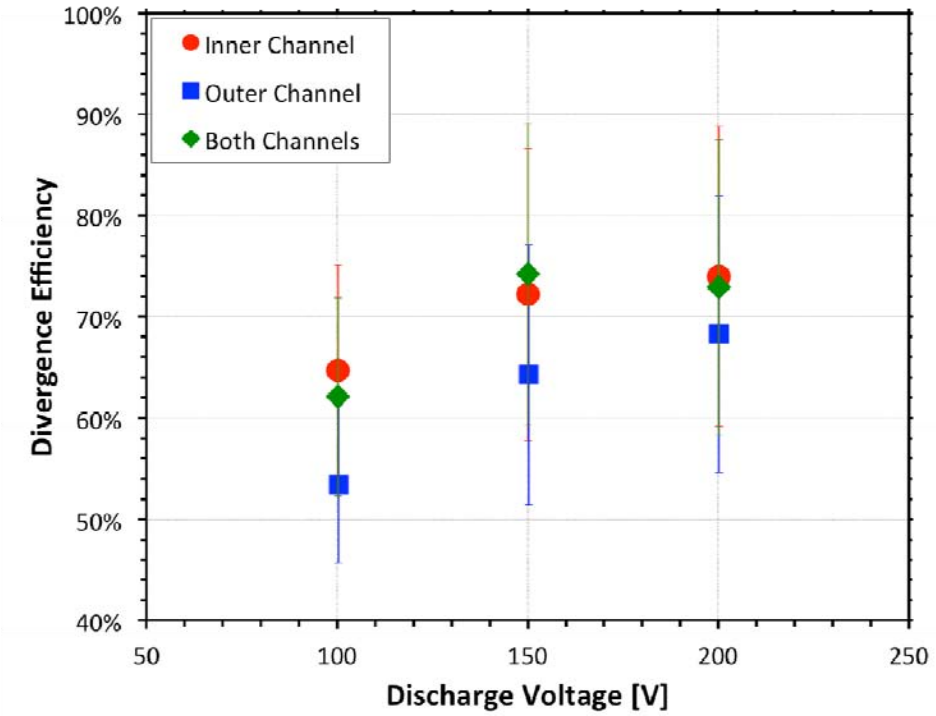

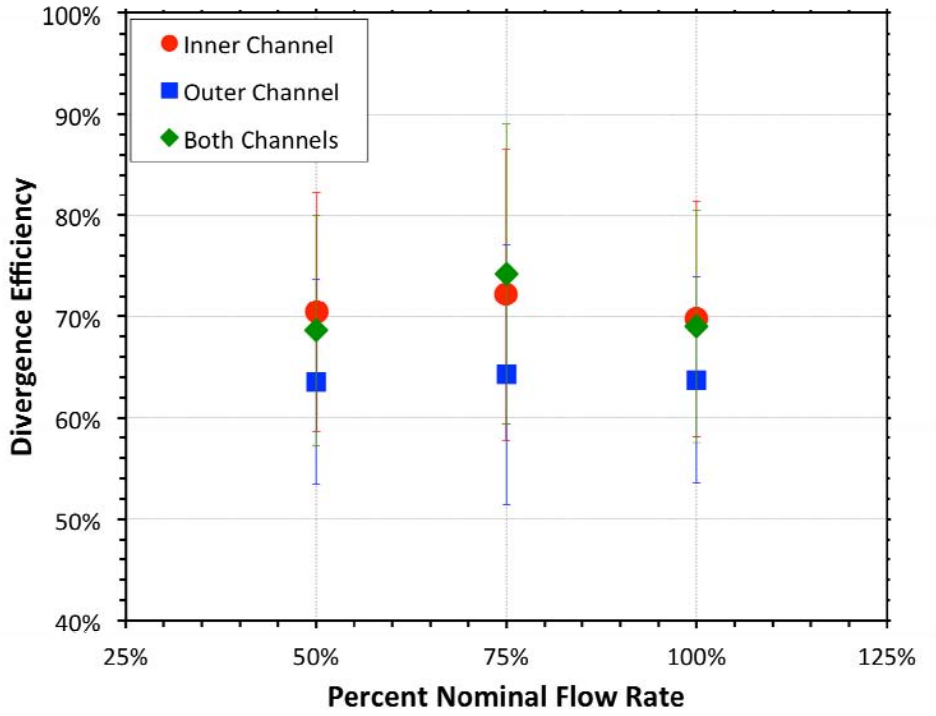

Charge Utilization Efficiencies

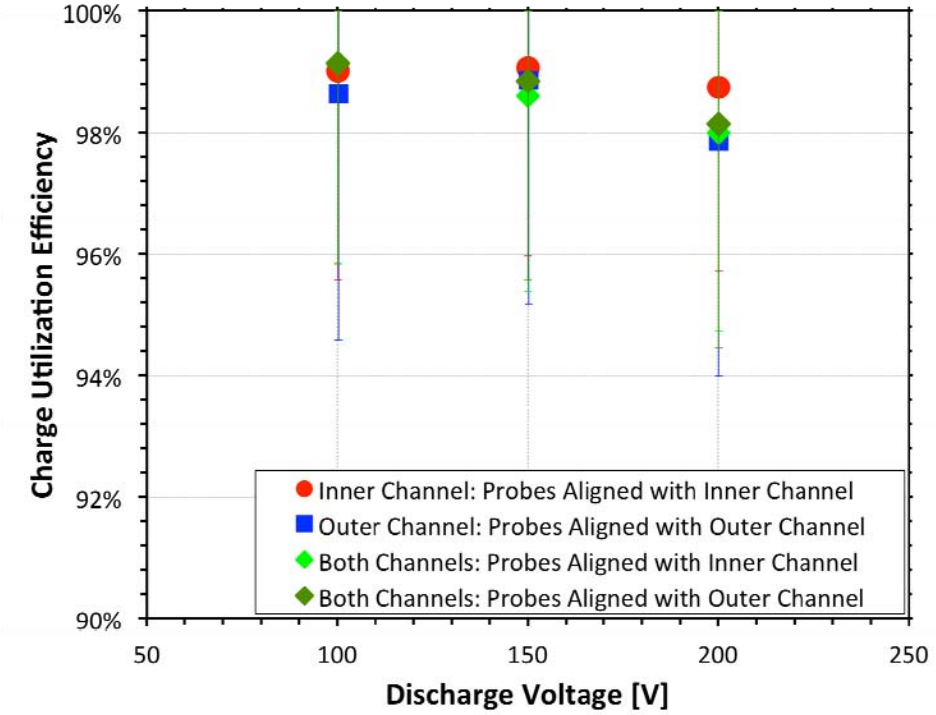

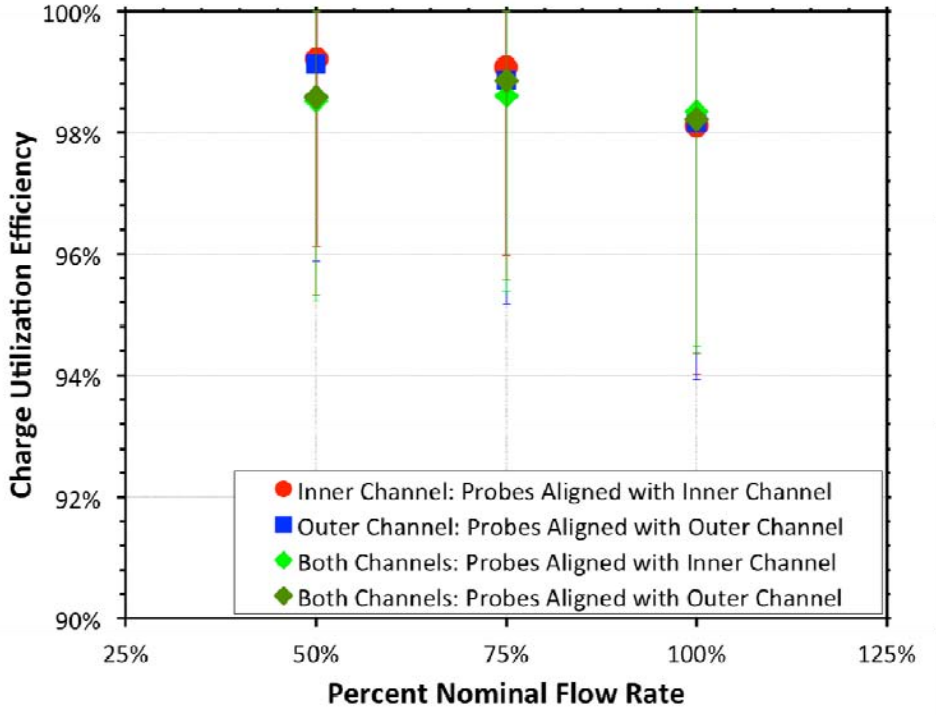

Mass Utilization Efficiencies

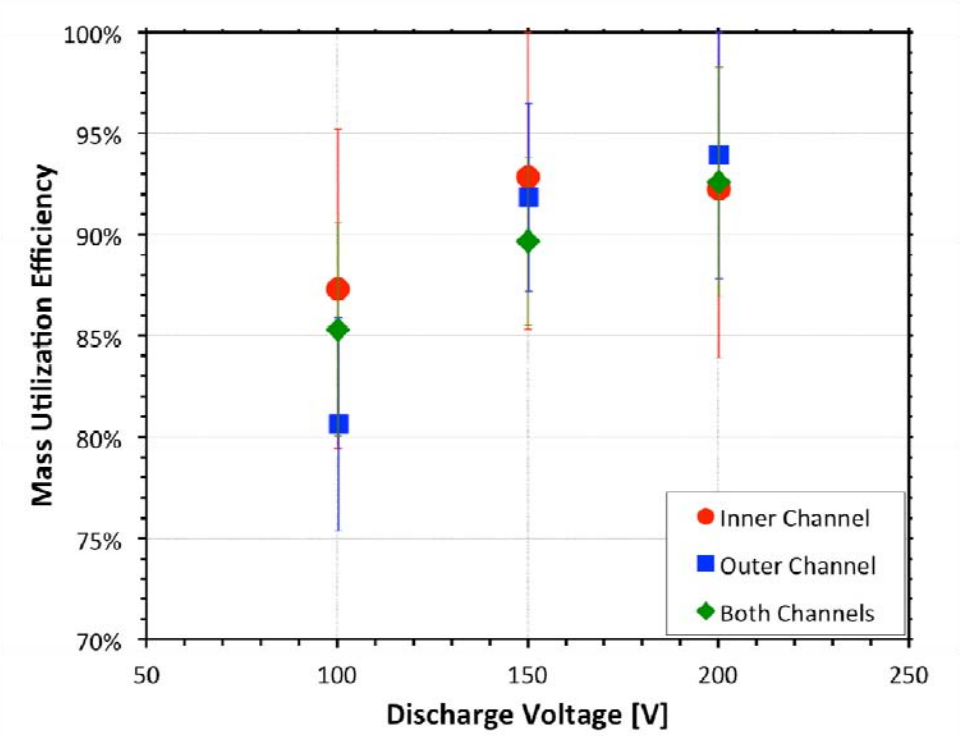

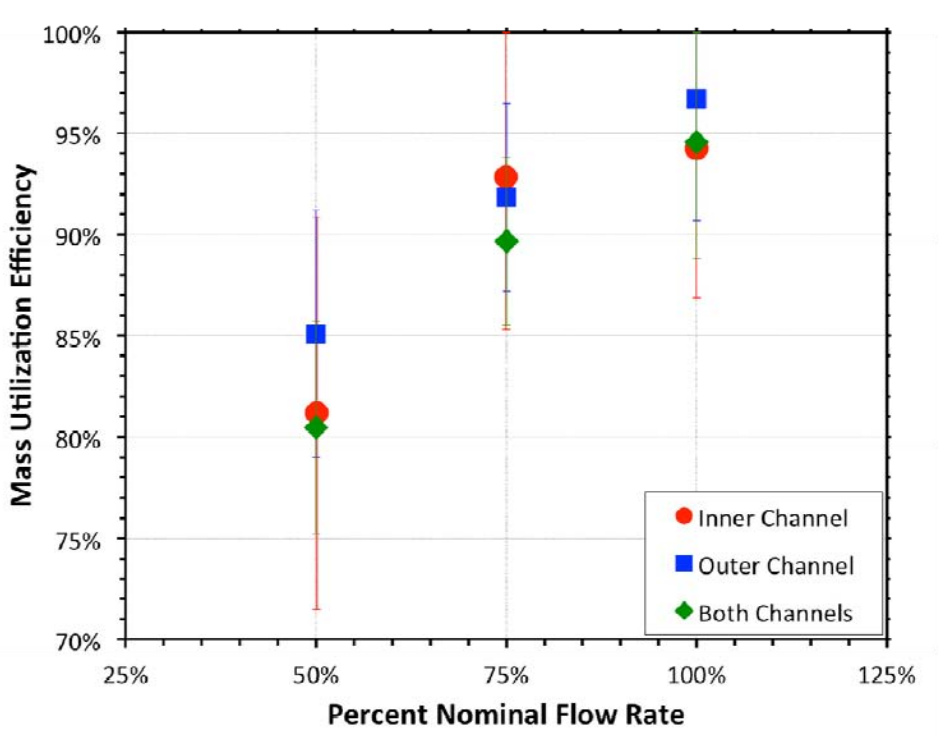

Voltage Utilization Efficiencies

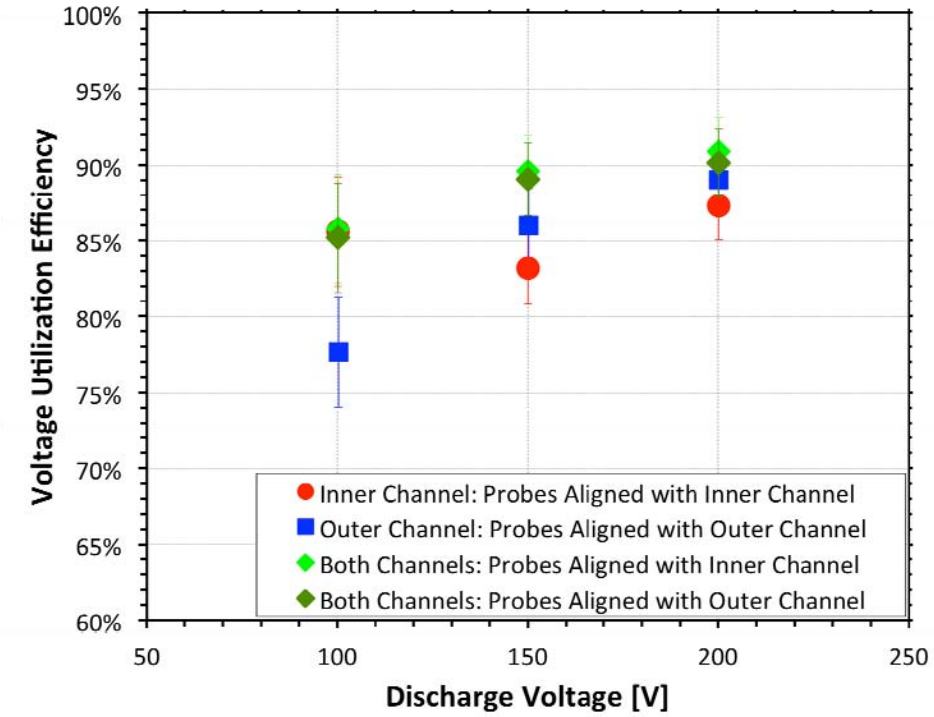

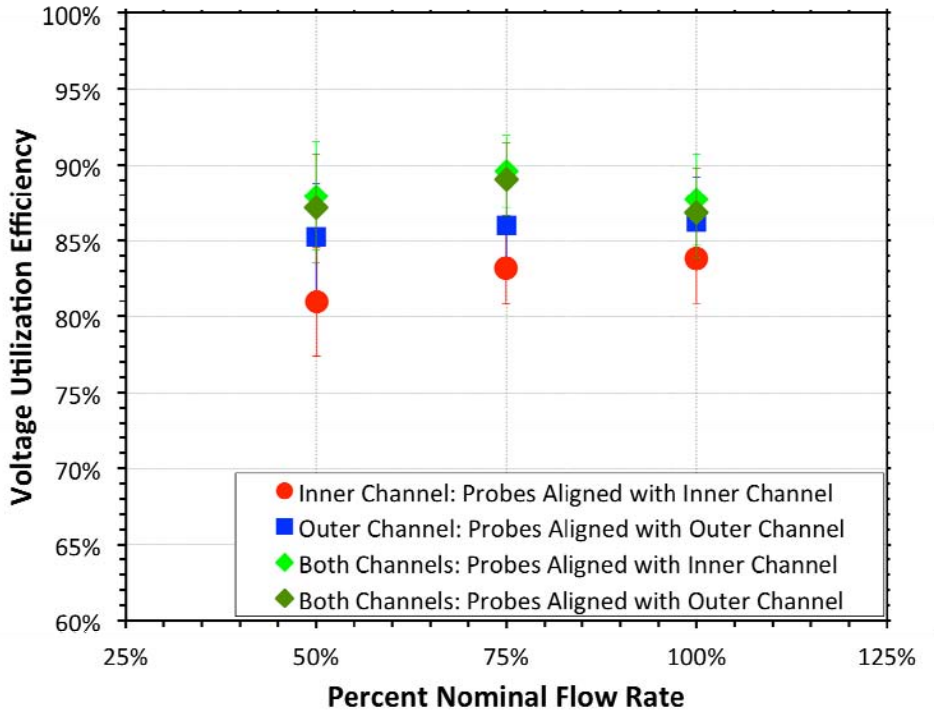

Cathode-Coupling Voltages

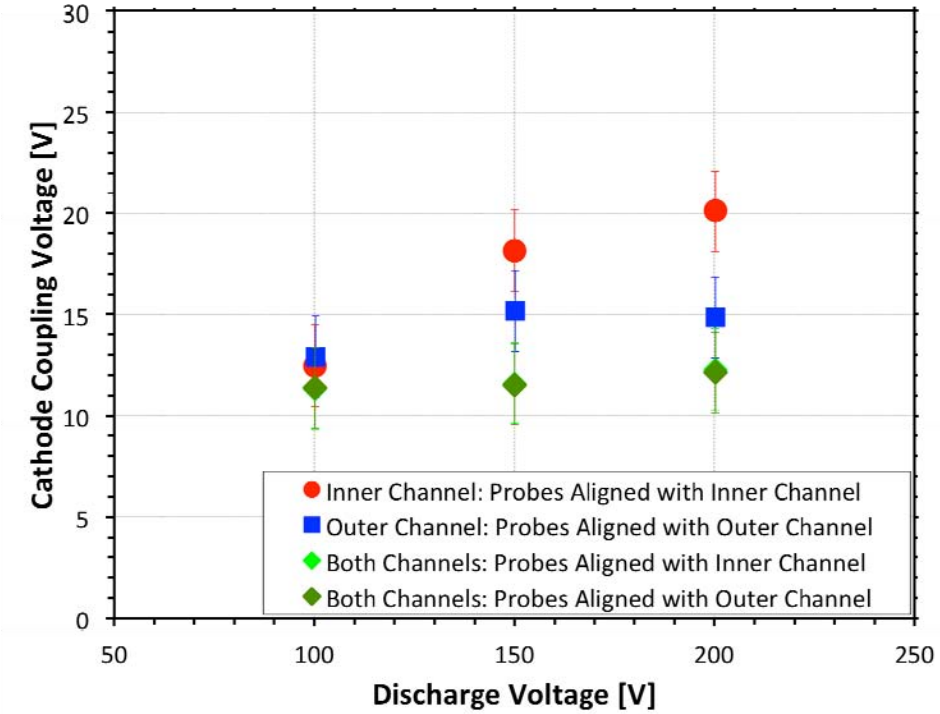

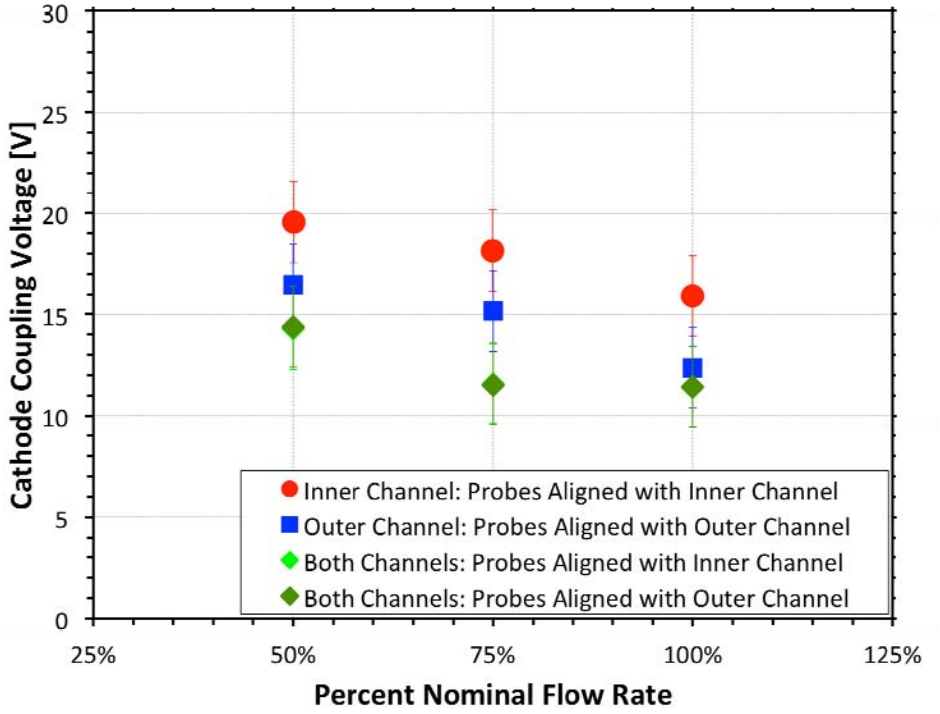

Total Efficiencies

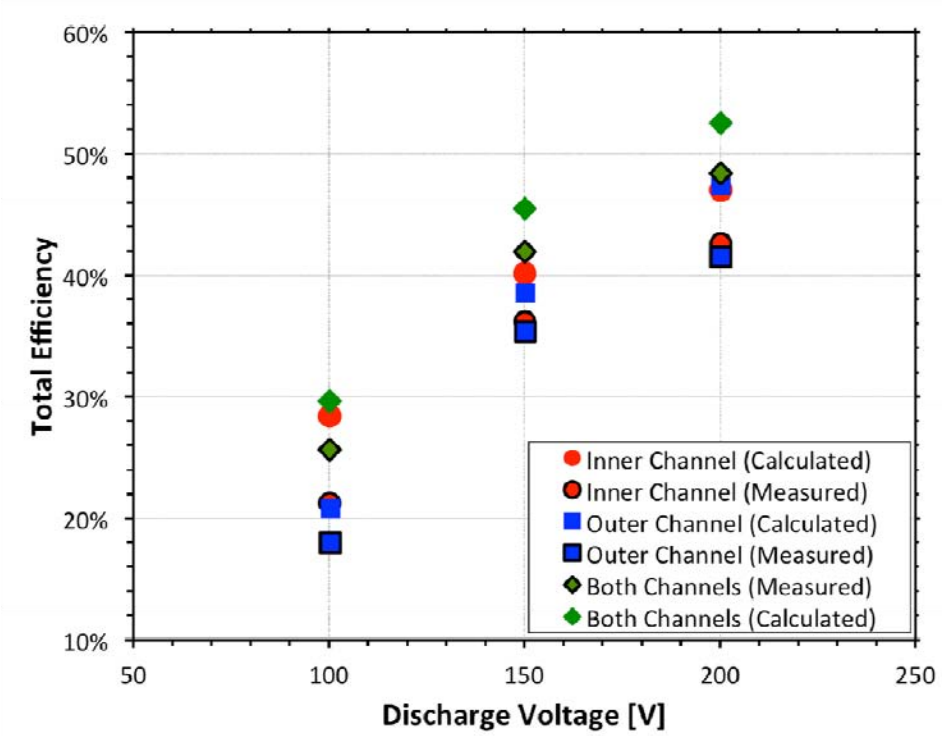

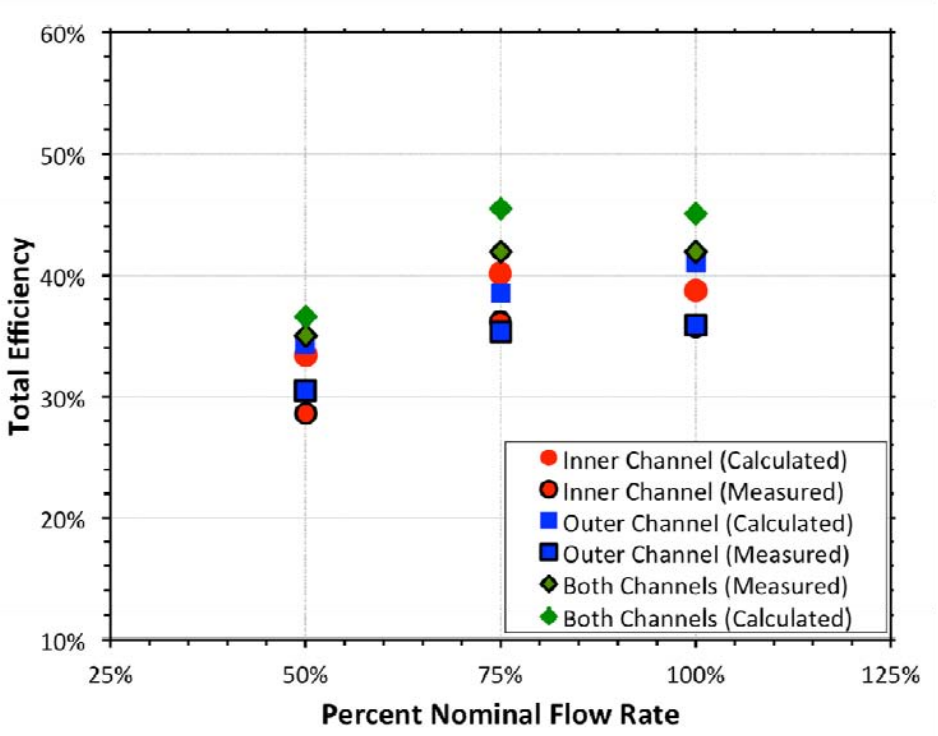

Conclusions

- The X2 NHT operates much like a conventional Hall thruster when both channels are at the same discharge voltage
- Increased voltage utilization and a decreased charge utilization in nested-channel mode
  - Further investigation on increasing this effect
  - Prompts more detailed measurements of the plasma potential distribution
- Current utilization, divergence, and mass utilization remain relatively constant between operating modes

Acknowledgements

- Our sponsors at the Air Force Research Laboratory
  - Dr. Daniel Brown
  - Dr. Brian Beal
  - Dr. James Haas
- AFRL for our new LaB_6 cathode and the RPA at PEPL
- National Defense Science and Engineering Graduate (NDSEG) Fellowship for supporting Raymond Liang

Appendix

Mixed Voltage RPA Measurements

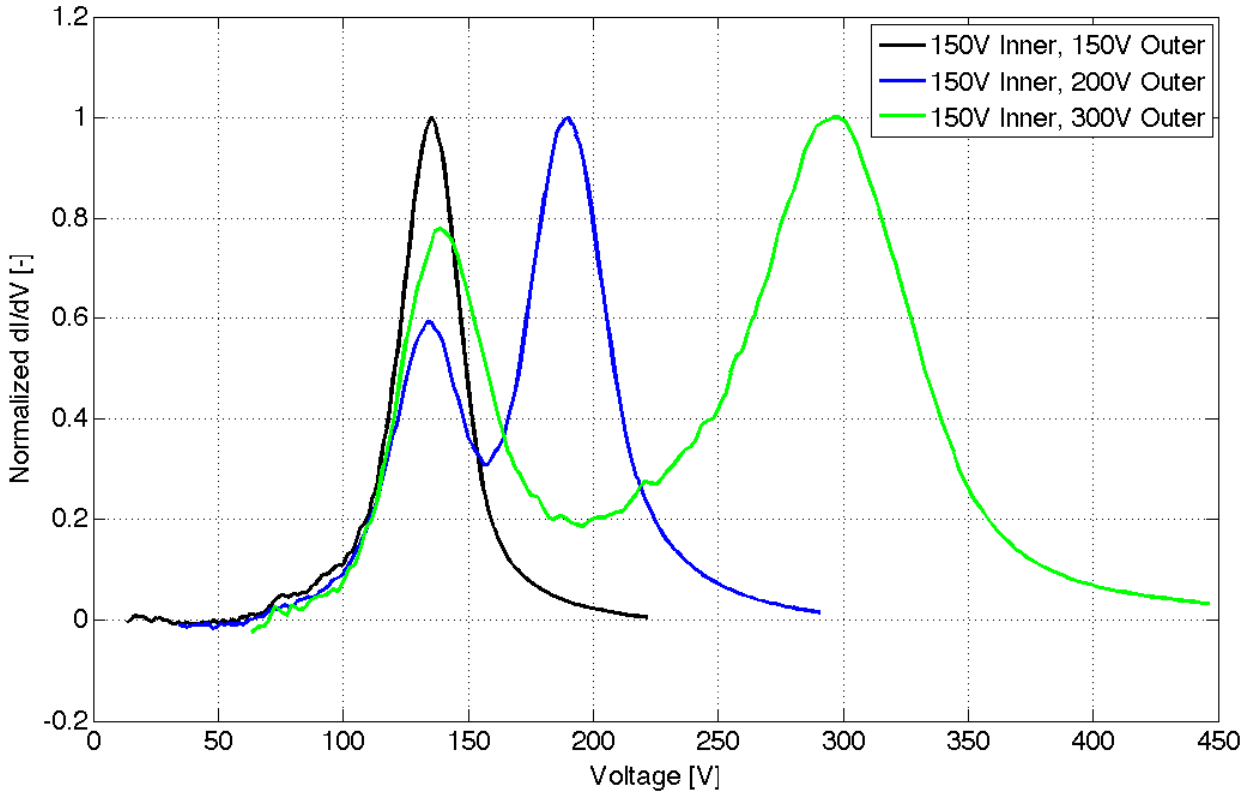

Mixed Voltage E×B Spectra

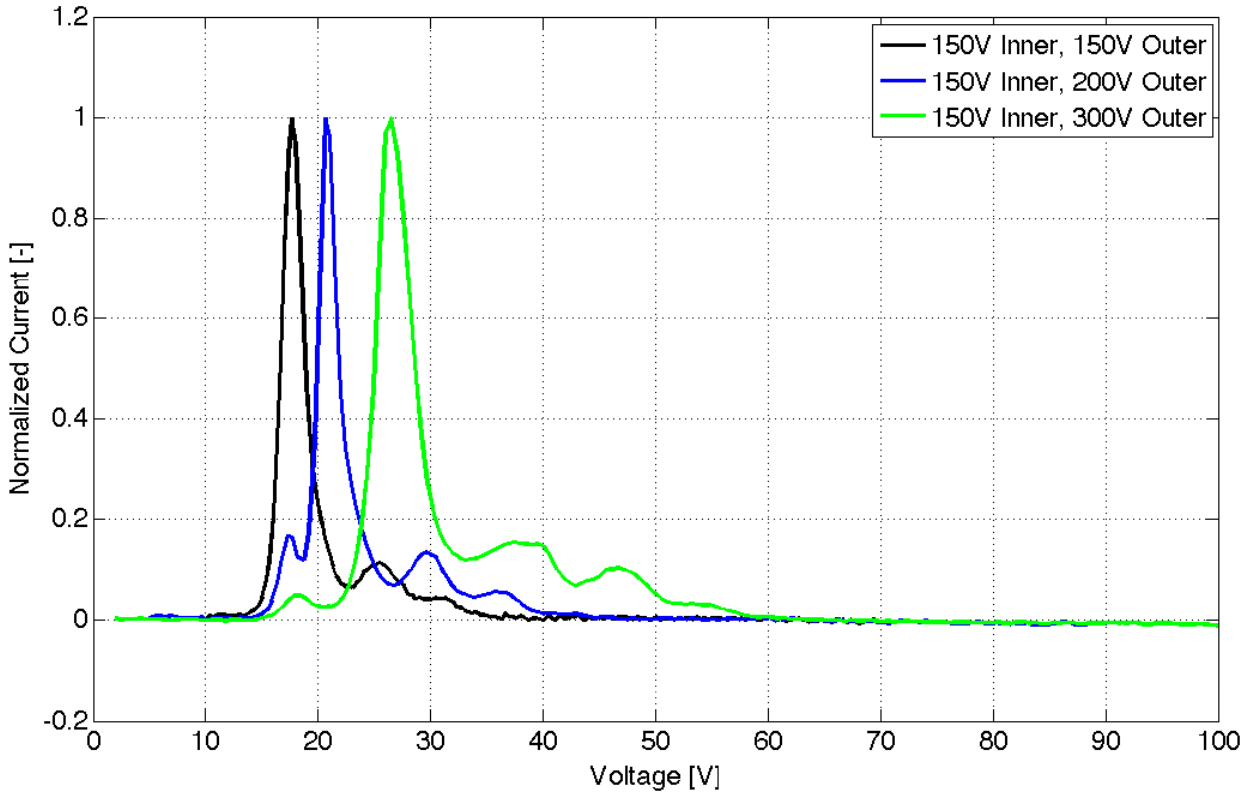

Mixed Voltage E×B Spectra

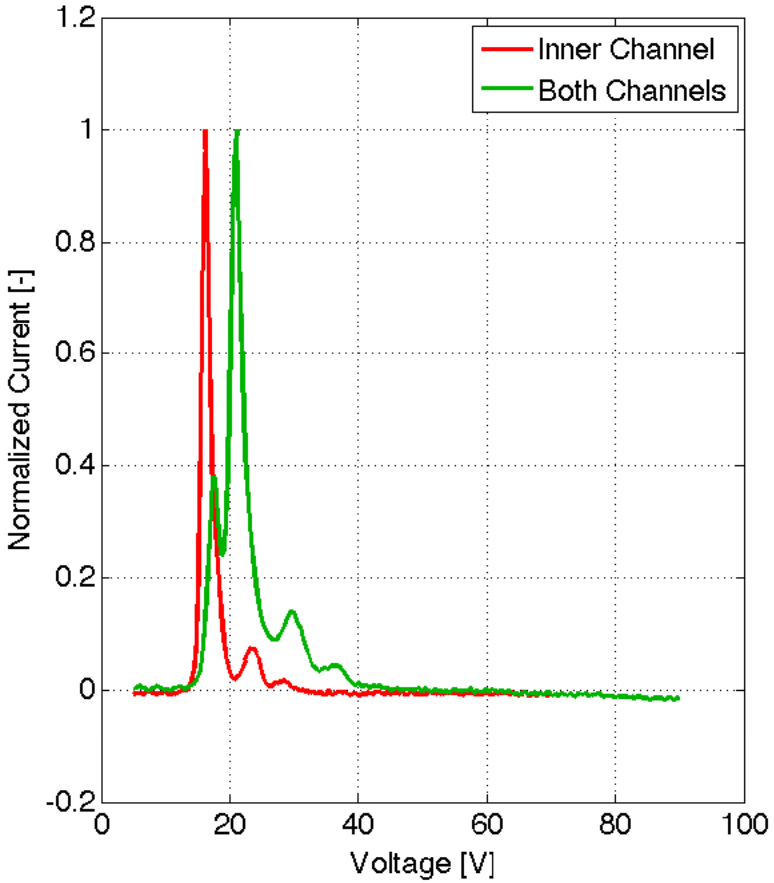

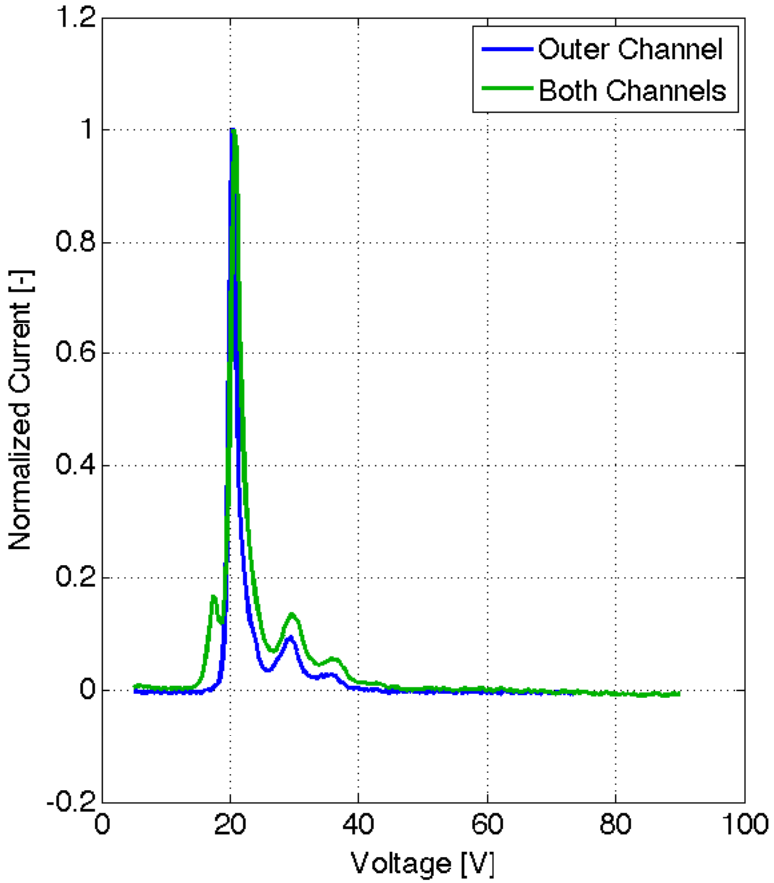

UNIVERSITY OF MICHIGAN